Nonlinear evolution of modified two stream instability above ionosphere of Titan: comparison with the data of the Cassini Plasma Spectrometer

Zoltán Dóbé and Karoly Szego
KFKI Research Institute for Particle and Nuclear Physics, Budapest, Hungary

Kevin B. Quest, Vitali D. Shapiro[1]
ECE Department, University of California San Diego, La Jolla, California 92093

Richard E. Hartle, Edward C. Sittler Jr.
NASA Goddard Space Flight Center, Greenbelt, MD 20771

[1] Also at Department of Physics, University of California San Diego, La Jolla, California 92093

Abstract. The ionosphere of Titan, moon of Saturn is directly exposed to the streaming plasma either of magnetospheric or solar wind origin. A turbulent interaction region between the two different plasma types is formed, called here flowside plasma mantle, where both ionospheric and hot streaming plasma are present at comparable densities. In order to study the microphysics of the collective plasma phenomena taking place within the flowside plasma mantle of Titan, a one dimensional electromagnetic hybrid simulation was constructed, retaining the inertia of the electrons. In the present paper it is shown that the excited waves are very effective in generating “anomalous viscosity” type interaction between the hot plasma flow and cold ionospheric ions, leading to significant bulk velocity loss of the proton component of the external plasma flow and turbulent heating of the ionospheric ions. The waves are excited due to a modified two-stream instability, the free energy source for the instability is in the streaming ion flow. The stochastic energy transfer from the streaming plasma to the ionospheric ions may also increase the tailward planetary ion escape by collective pick-up mechanism enhancing the rate of erosion of the atmosphere of Titan (sputtering). We make predictions for the characteristic frequency range and saturation energy level of the excited wave electric field, and the energy range where superthermal charged particles of ionospheic origin can be detected by the charged particle analyzers onboard of Cassini spacecraft near Titan.

1. Introduction

The interaction of the solar wind with non-magnetized planetary bodies (such as Mars and Venus) has long been a subject of great scientific interest, and our knowledge about this interaction has been greatly enhanced since the Pioneer Venus mission. At Mars the results of the Phobos space mission, the Mars Global Surveyour Mission, and recently Mars Express contributed with exciting data. According to our current understanding, in both cases the obstacle of the solar wind is a relatively thin, induced magnetic barrier just above the ionopause (the upper edge of the ionosphere) at Venus, and above the very likely diffuse ionosphere boundary at Mars. It has been shown [*Spereiter and Stahara*, 1985] that around such an obstacle the shocked solar wind slows down as we approach the obstacle, flows around the tangential discontinuity formed by the ionopause. This "simple" picture has become complicated by several processes. Ions of planetary origin diffuse through the ionopause boundary, or get released at the exobase. These ions interact with the shocked solar wind leading to various loading mechanisms [c.f. *Szego et al*., 2000a].

One is the $E \times B$ pickup, when the new ions are accelerated by the local ambient field and are starting to gyrate around the magnetic field. The gyroradius depends on the strength of the local magnetic field, therefore the $E \times B$ loading has different effects as we move away from the Sun. The new ions add mass to the flow, and takes momentum and energy from it, therefore they increase the deceleration process.

There is an other effect when the escaping ions excite waves in the surrounding shocked solar wind flow, and the waves heat and accelerate the planetary ions within a relatively narrow region above the ionosphere. The existence of such ions around Venus has been shown by *Grebowski et al*., [1993]. This second type of mass loading was termed as "laminar pickup" or "sputtering" to emphasize that this process

operates only in the near environment of ionosphere. This is the mechanism we address in this paper.

The close proximity of the barrier to the planetary atmosphere results in direct contact of the shocked solar wind plasma with that of the ionosphere, and the coupling that results is quite distinct from the observed in the Earth's magnetospheric system. The formation of a transition region between the planetary ionosphere and solar wind, called dayside plasma mantle, was identified by the different plasma instruments onboard of both the Pioneer Venus Orbiter [*Spenner et al*., 1980; *Scarf et al*., 1980; *Taylor et al*., 1981; *Szego et al*., 1997] and Phobos 2 [*Lundin et al*., 1989; *Riedler et al*., 1989; *Rosenbauer et al*., 1989] spacecrafts. Based on these measurements one can conclude that within the Venusian and Martian mantle both the shocked solar wind and planetary plasma are present in comparable densities within a region 100-200 km above the ionopause/planetopause, and the shocked solar wind decelerates behind a so called mass loading boundary due to the presence of the cold planetary ions. The bulk of the shocked solar wind protons are deflected above the mantle while the total magnetic field increases and a magnetic barrier is formed (*Zang et al.,* [1991]). Intense electrostatic wave activity was observed in the vicinity of and somewhat above the local lower hybrid frequency. Superthermal planetary ions (in the energy range of few ten eV) and electrons (in the energy range of few 100 eV) were also observed within the dayside mantle of Venus and Mars.

Titan, moon of Saturn, in many respects is very similar to Venus and Mars. It has negligible intrinsic magnetic field and has also a dense ionosphere which is produced by the photoionization by the solar extreme ultraviolet photons and energetic electrons originated from the Saturnian magnetosphere. Depending on its orbital position and solar wind conditions Titan may be located either within the magnetosphere of Saturn, or during increased solar wind ram pressures may cross the

magnetopause or even the bow shock entering into the magnetosheath/tail region of Saturn or the unperturbed solar wind, respectively.

The first *in situ* measurements of the plasma environment of Titan were provided by the particle and field instruments onboard Voyager 1 when Titan was located within the magnetosphere of Saturn; and Voyager 1 crossed the tail region of Titan. According to these measurements (*Hartle et al*., [1982]; *Ness et al*., [1982]; for a review see *Neubauer et al*., [1984] and *Neubauer* [1992]) the magnetospheric plasma was composed of H^+ and N^+ or O^+ ions, with characteristic densities of 0.1 and 0.2 cm^{-3} and Voyager 1 investigators reported temperatures of about 210 eV and 2.9 keV proton and heavy ion temperatures, respectively. The temperature of the magnetospheric electrons in the neighborhood of Titan was of the order of 200 eV. The characteristic ion flow speed outside the wake of Titan was ~120 km s^{-1}, and the magnetic field is of the order of 5 nT. Based on these parameters one can conclude that the flow is subsonic (sonic Mach number $M_S \sim 0.6$) and trans-Alfvénic (Alfvénic Mach number $M_A \sim 1.9$). The analyses of the Voyager 1 data gained in the wake of Titan showed a complex interaction between the upper atmosphere of Titan and the magnetosphere of Saturn, where the finite gyroradius effects are essential, resulting in asymmetric removal of ions from the Titan's upper atmosphere. The major ionization sources of Titan's neutral corona are photoionization, electron impact ionization and charge exchange (see for e.g. *Nagy and Cravens*, [1998]), the structure of Titan's ionosphere inside the magnetosphere being dependent on the relative angle of the directions of the particular ionization process. The presence of pickup ions near Titan was detected by the plasma science instrument during inbound approach. Recently, Sittler and coworkers (see *Sittler et al.*, [2004] and *Sittler et al*., [2005]) revisited the Voyager 1 results, and concluded that the light pickup ions H^+ and H_2^+ dominate in the outermost region with respect to Titan's "ionopause", followed by CH_4^+ at intermediate distances and the plasma flow experienced major mass-loading effect

when it reached the region just outside the "ionopause" dominated by heavy ion species such as N_2^+.

The particle and electromagnetic field measurements of the Cassini spacecraft performed in the wake region of Titan during the six fly-bys between October 26, 2004 and August 23, 2005 confirmed most of the earlier plasma observations Voyager 1, however, important new features were also observed in the plasma environment of Titan.

Within the magnetosphere, outside the interaction region of Titan, the presence of light and heavy ion populations, predominantly protons and 16AMU (O^+ and/or CH_4^+) ions were identified by Cassini Plasma Spectrometer (CAPS) (*Crary et al.*, 2005). Characteristic ion flow speeds varied around 110 ± 20 km/s, with protons and heavy ion temperatures of ~250 and 1000 eV, respectively. Magnetospheric electron density varied roughly an order of magnitude, centered around ~0.1 cm^{-3}, with temperatures typically between 50 and 200 eV. Also based on CAPS data, *Szego et al*. [2005] identified four major regions in the plasma environment of Titan, the outermost characterized by the appearance of unperturbed corotating flow, closer to Titan pickup ions started to appear probably due to local pickup. After that the flowing magnetospheric plasma was significantly decelerated, and the last region above the ionosphere was characterized by a cold plasma population of planetary origin. The ions in this fourth region have many similarities to the ion population observed by PVO above the ionosphere [*Grebowski et al.*, 1993]. The heavy ions of the undisturbed corotating flow show characteristics which are different from a beam-like distribution, though very likely they do not form a homogeneously filled shell distribution. The measured proton spectra indicate a cooler proton population than reported by the Voyager 1 investigators.

While approaching Titan Cassini entered into the so called mass-loading region where ions originating from Titan's neutral corona and/or from its ionosphere were

detected by both CAPS and Cassini Radio and Plasma Wave Science (RPWS) Langmuir Probe (LP) sensors (*J.–E. Wahlund et al.*, [2005]). In this region the cold ions are being accelerated and picked up by the streaming magnetospheric plasma, and at the same time due to the momentum exchange caused by the ionospheric ions accommodated into the magnetospheric ion flow slows down to drift velocities of order of few km s^{-1}, while the electron density increased during both inbound and outbound passes of the spacecraft. The deceleration region was substantially asymmetric during all flybys, more extensive on that side of Titan where the $V \times B$ electric field pointed away from the moon, a feature suggesting the importance of the finite Larmor radius effects. Based on CAPS data, *Hartle et al.* (2005) showed that the heavy ambient ions, mainly O^+ and/or CH_4^+, observed within the ambient magnetospheric plasma flow are absent in the mass loading region of Titan, being probably removed by the extended atmosphere of Titan also due to the relatively large gyroradius of these ion species. The pickup ion component detected within the mass loading region were identified as H^+, H_2^+, N^+/CH_2^+, CH_4^+, and N_2^+, where the ~28AMU type ions do most of the mass loading.

Magnetic enhancements (pileup), magnetic field line draping and magnetic ionopause layer were also detected within the mass loading region of Titan (*Backes et al*., [2005]), similarly to the corresponding regions of Venus and Mars. Also confirming the earlier Voyager 1 results, no evidence of internal magnetic field at Titan was detected by the magnetometer of Cassini. Near the closest approach of Titan, at altitudes about 1250 km, the RPWS Langmuir probe measured maximum plasma desities of the order of 2000 to 4000 cm^{-3}, and electron temperatures ranging from 110 to 1400 K.

According to CAPS ionospheric plasma composition measurments performed below 1650 km altitude range (*Crary et al.*, 2005) the strongest density peak was assigned to the 28AMU ions. Based on models of Titan's ionospheric chemistry, this could

probably be $HCNH^+$, $C_2H_5^+$ or N_2^+. Minor ion species of higher mass were also found with ~12AMU spacing between these peaks, characteristic of heavier hydrocarbons. A numerical simulation of the Titan flyby's shows that the interaction region is asymmetric w.r.t. the corotation flow direction (Chanteur et al, 2005), and yet unpublished results indicate two important features of the mass loaded regions: a)The the corotating flow itself has certain variability, b) in the wake region of Titan the heavier component of the corotating flow is often not detected (www.caps.swri.edu).

Several MHD models (*Keller et al.*, [1992], *Roboz and Nagy*, [1994]; *Cravens et. al*., [1998]; *Ledvina and Cravens*, [1998]; *Kabin et al*., [1999], *Nagy et al*., [2001],) and kinetic type models (*Brecht et al*., [2000]; *Kopp and Ip* [2001]; *Ma et al.*, [2004]; *Kallio et al.*, [2004]) have been developed in the last decade in order to improve our understanding of the large scale structure and formation of induced magnetosphere and plasma environment, including the ionosphere of Titan.

It is straightforward to assume that due to the direct contact between streaming plasma of magnetospheric or solar wind origin and the ionospheric plasma of Titan an interaction region similar to the dayside plasma mantle of Venus and Mars is formed. In what follows, by analogy, we call this region the flowside plasma mantle of Titan. Theoretical studies support the idea that significant collisionless momentum and energy exchange is taking place in this transition region due to wave-particle interaction, resulting in a highly turbulent layer, where even the bulk properties of the of the plasma would significantly change due to this so called "anomalous viscosity" [*Sagdeev et al.*, 1990]. In contrast to the mass loading of the flow which is significantly influenced by the direction of the $V \times B$ electric field, as the result of the wave particle interaction itself the two sides of Titan are identical, however, any asymmetry of the interacting flow will cause asymmetric effects. Two types of instability modes were proposed as explanations of the observed wave activity in the Venus and Mars plasma mantle: the lower hybrid drift and modified two stream

instability with typical frequencies in the vicinity of the lower hybrid frequency and wavelength of the order of solar wind electron gyroradius; [*Szego et al*, 1991; *Shapiro et al*, 1995; *Quest et al*., 1997, *Dóbé et al*, 1999]; and a beam resonant instability branch of ion acoustic type waves [*Huba*, 1994] with frequencies of the order of ionospheric ion plasma frequency, and typical wavelength of order of electron Debye length. *Szego et al*., [2000b] analyzed the robustness of the ion acoustic scenario and showed that the presence of even a small amount of cold planetary electrons quenches this mode.

In an earlier paper *Dóbé and Szego*, [2005] investigated the linear properties of the instability modes viable within the flowside plasma mantle of Titan. According to this study the fastest growing plasma waves possibly excisted within the flowside plasma mantle of Titan correspond to "lower hybrid" and the ion acoustic type modes generated by modified two stream instabilities (see ex. *Wu et al*., 1983; *Shapiro et al*., 1995) and ion-ion acoustic beam instabilities (see ex. *Gary and Omidi*, 1986), respectively. The modified two stream instability modes have frequencies and growth rates in the lower hybrid frequency range with wavelength between the electron and the ion gyroradius and propagate nearly perpendicular to the magnetic field. The ion-ion acoustic instability is a shorter wavelength (order of hot proton Debye length) and higher frequency (order of ion plasma frequency) electrostatic mode. *Dóbé and Szego*, [2005] performed a parametric study of these instabilities within the framework of the linear Vlasov theory of the plasma instabilities. Using a wide range of the plasma parameter space which enclosed the plasma measurements of Voyager 1 and the available model calculation, they made prediction concerning the characteristic frequencies and the spatial location of the dominant wave modes measurable by the plasma wave instrument onboard the Cassini spacecraft. It was shown that in the electrostatic limit the ion acoustic mode smoothly transforms into lower hybrid mode when the relative number density ratio of cold electrons becomes

comparable to or less than 10^{-2}. This means that the two dominant instability types can only exclusively be present in well separated spatial regions determined by the presence / absence of cold ionospheric electrons.

In the present study we focus on the nonlinear development of the MTSI mode using hybrid simulation methods. The paper is organized as follows: In section 2. detailed description of the of the simulation model is presented. In section 3. first we have demonstrated that the numerical simulation results match the analytical solution of the linear theory reasonably well in the appropriate domains, then examined the time evolution of the wave energy and bulk plasma characteristics such as momentum and thermal energy of the different plasma components, determined typical ion energy spectra formed as a result of nonlinear wave particle interaction, and made predictions for Cassini electric field and plasma probe measurements. In section 4. we have explored in more details the mechanisms of collisionless coupling between the streaming and stationary plasma, including the microscopic details of the acceleration processes and turbulent plasma heating induced by the MTSI instability. The effective collision frequency between the streaming plasma and ionospheric ions that characterize planetary ion pickup and heating have also been calculated. In section 5. we have compared some elements of our model result with data measured by Cassini's Plasma Spectrometer. Finally, in section 6. we have summarized the main conclusions of our present study.

2. Model description

In order to investigate the collisionless interaction between the streaming plasma of Saturnian magnetosphere or solar wind origin and ionosphere of Titan mediated by MTSI a one dimensional electromagnetic hybrid particle-in-cell simulation has been

constructed. The simulation model treats the ion species using particle-in-cell (PIC) methods. The ions approximated as macroparticles are moved using standard time-centered leapfrog algorithms, with ion density and current collected at the corners of a rectilinear grid. Given these source terms, the electromagnetic fields are also solved on the grid, with which the ions are moved during the next time step. The field equations are solved using the predictor-corrector method described in *Quest*, [1989]. On the other hand the electrons are modeled as charge neutralizing, adiabatic fluid in which inertial and electromagnetic effects are retained. The electromagnetic field quantities are then advanced by solution of a coupled set of linear partial differential equations. All vector physical quantities are kept three dimensional, however, their spatial dependence was constrained to one dimension, parallel to the wave propagation direction. Periodic boundary conditions are imposed, and the initial system is allowed to relax in time. Besides the local charge neutrality, another natural consequence of the one dimensional hybrid PIC simulation model with periodic boundary conditions is the current neutrality condition (*i.e.* zero net electric current density in the flow direction). The particle initialization is performed by imposing relative drift between uniformly distributed Maxwellian protons / 14-16 AMU ions, corresponding to the magnetospheric plasma, and stationary ionospheric ions.

The first PIC-type description of the plasma wave generation within the interaction region of nonmagnetic planets with substantial atmosphere such as Mars and Venus was given by *Quest et al.*, [1997], where the bulk velocity of the streaming plasma was constricted to direction strictly perpendicular to the ambient interplanetary magnetic field. This model was further developed by *Dóbé et al*., [1999] allowing for arbitrary although fixed wave propagation direction with respect to the external magnetic field lines.

It was straightforward to extend the investigation of *Dóbé et al*., [1999] for the case of interaction of Titan's ionosphere with the streaming plasma of Saturnian

magnetosphere or solar wind origin. In a preceeding paper *Dóbé and Szego*, [2005] has already discussed the possible beam driven linear wave generation mechanisms viable within the flowside mantle of Titan. In this work the general form of the linear dispersion equation of the cross-magnetic field beam instabilities for the low frequency limit (derived by *Wu et al*, [1983]) was solved for a large plasma parameter range relevant to the plasma mantle of Titan. Low frequency here means that $\omega_{ci} << \omega << \omega_{ce}$, where $\omega_{c(i,e)} = eB_0/m_{(i,e)}c$ are the gyrofrequency of the ions – $i = p$ (protons), N^+ / O^+ (nitrogen or oxygen ions) and I (ionospheric ions) – and electrons (e), respectively. In this limit the electrons were taken as magnetized, while ions as unmagnetized charged particles. (The notion "unmagnetized" in this sense means that the characteristic wavelength of the instability is much smaller than the ion gyroradius and the characteristic frequency and increment of the instability is much larger than the ion gyro-frequency.) It was shown that in the presence of cold electrons of ionospheric origin (even in a ratio of order of 1% of the total plasma density) the fastest growing waves are generated by the modified two-stream instability (MTSI) driven by the non-resonant interaction between the unmagnetized ionospheric ions and the cold, magnetized electron beam created by fast $E \times B$ pickup. Pickup of the cold electrons originating from the ionospheric plasma of Titan, by analogy with the case of the dayside mantle of Venus and Mars described by *Dóbé et al*., [1999], takes place over a few electron gyroperiods, a time interval much shorter than the lower hybrid period, characteristic time scale for the MTSI waves. Although the cold electron beam has little kinetic energy of its own, the wave-particle resonance is sustained for a longer time due to electron pickup under the combined action of the magnetic and convective electric field of the solar wind. This makes possible a substantial transfer of free energy from streaming plasma flow to the waves already at the initial linear wave growth stage. It has also to be mentioned that the bulk velocity of cold pickup electrons at each time step of the simulation is

determined by the zero net current condition , $\mathbf{u_e} = \Sigma_i(n_i/n_e)\ \mathbf{u}_i$, where n_i, n_e and $\mathbf{u}_i$, $\mathbf{u_e}$ are the number densities and bulk velocities of ions and electrons, respectively. It can be easily proven that releasing the condition of zero net current in the analytic dispersion relation does not alter the evolution of instability, at least in its linear stage.

In Figure 1. we have presented a schematic illustration of the simplified physical model used in our one dimensional hybrid PIC simulation model similar to the one used during the linear model calculations of *Dóbé and Szego*, [2005]. The upper panel shows a sketch of the flowside plasma environment of Titan. The hot plasma flowing past the moon with drift velocity $\mathbf{U_{beam}}$ interacts with the cold plasma of ionospheric origin in the presence of the external magnetic field, $\mathbf{B_0}$, creating the plasma mantle. The drift velocity of the flowing plasma is deflected due to the interaction and becomes gradually parallel within the plasma mantle with the upper boundary of the ionosphere. Meanwhile the external magnetic field frozen into the plasma flow drapes the obstacle and piles up, forming the so called magnetic barrier. The lower panel shows the orientation of the coordinate system used in the model calculations. Without loosing generality we can take the wave number vector **k** parallel to *Ox* and $\mathbf{B_0}$ laying within the *Oxz* plane. The characteristic length of the simulation box was choosen to be 32 times the characteristic wavelength of the MTSI instability corresponding to the linear growth stage (90-160 km).

It can be easily shown that in the cold, magnetized electron limit – that is when the electron resonance term $w_e \equiv (\omega - \mathbf{k}\mathbf{u}_e)/\sqrt{2}k_{\|}v_{Te} >> 1$ – the fluid approximation is appropriate for electrons. Here we introduce the standard notations: $v_{T(i,e)} = (k_B T_{(i,e)}/m_{(i,e)})^{1/2}$ is the thermal velocity; $\mathbf{u}_i$ and $\mathbf{u}_e$ are the drift velocity vectors, T_i and T_e are temperatures, m_i and m_e are masses corresponding to the different ion species and electrons, respectively; $k_{\|}$ is the component of the wave vector **k** parallel to the external magnetic field $\mathbf{B}_0$; k_B is the Botzmann constant. $\omega_{p(i,e)} = (4\pi e^2 n_{(i,e)}/m_e)^{1/2}$ are the plasma frequencies, $\lambda_{(i,e)} = (k_B T_{(i,e)}/4\pi n_{(i,e)} e^2)^{1/2}$ are the Debye length, n_i and n_e are

the densities of the ion or electron components, respectively. Here we also introduce the lower hybrid frequency , which in the dense plasma case ($\omega_{pe}^2 >> \omega_{ce}^2$) valid within the plasma mantle of Titan can be approximated as $\omega_{LH} \approx (\omega_{cp}\omega_{ce})^{1/2}$. Using single temperature Maxwellian, unmagnetized ion velocity distributions for the unperturbed particles the general dispersion relation (equation (1) in *Dóbé and Szego* [2005]) simplifies to the form:

$$\left(1+\frac{\omega_{pe}^2}{k^2c^2}\right)\left(\frac{\omega_{pe}}{\omega_{ce}}\right)^2-\left(\frac{\omega_{pe}}{\omega-\mathbf{ku_e}}\right)^2\frac{k_{\|}^2c^2}{k^2c^2+\omega_{pe}^2}+\sum_{p,N+,I}\frac{1}{k^2\lambda_i^{\,2}}\left[1+w_iZ(w_i)\right]=0 \qquad (1)$$

Here $Z(\xi)$ is the plasma dispersion function: $Z(\xi) = i\sqrt{\pi}\exp(-\xi^2)\,[1 + erf(i\xi)]$, where *erf* is the error function; the unmagnetized ion resonance terms are of the form $w_i \equiv (\omega - \mathbf{k}\cdot\mathbf{U}_i)/\sqrt{2}kv_{Ti}$. A similar form of of the MTSI dispersion relation (1) was obtained and extensively discussed for the Venus case by *Shapiro et al.*, [1995].

The mechanism of the dominant instability branch is similar to the well known Buneman-instability. In our case the Doppler shifted wave frequency within the electron beam, $\omega - ku_e$ becomes resonant with one of the plasma eigenmode, the whistler mode, according to the resonance condition: $kU_e = \omega_{ce}k_{||}kc^2/(k^2c^2+\omega_{pe}^2)$. As already discussed in a previous paper by *Dóbé and Szego*, [2005] the approximated solution of (1) for the most dominant mode is:

$$\omega_r + i\gamma \approx \left(\frac{1}{2}\right)^{4/3}\left(\frac{n_i}{n_e}\right)^{1/3}\left(\frac{m_p}{m_I}\right)^{1/3}\kappa^{1/3}(1+i\sqrt{3})\omega_{LH} \qquad (2)$$

where $\kappa = (k_{||}/k)\sqrt{(m_p/m_e)}$ corresponds to wave propagation angles relative to the magnetic field, $\theta = \arccos[\kappa\sqrt{(m_e/m_p)}]$, and the effect of the protons and nitrogen /

oxygen ions onto the evolution on the instability – at least in the linear stage – is negligible.

3. Model results

3.1 Linear growth phase of the MTSI

First, we show that the result of the numerical simulation is "correct" that is it matches reasonably well the analytical solution of the linear theory in the appropriate domains. This is shown in Figure 2. Here we have solved the dispersion relation (1) using average plasma parameters close to the ones measured by Voyager-1 in the plasma wake of Titan [*Hartle et al.*, 1982]: U_b = 120 *km/s*, n_p=0.1 cm^{-3}, $n_{N/O+}$=0.2 cm^{-3}, T_p = 210 *eV*, $T_{N/O+}$ = 2.9 *keV*. These plasma density and temperature values are close to the ones measured by the Cassini ion mass spectrometer (*Crary et al.*, [2005]; *Hartle et al.*, [submitted to *Geophys. Res. Lett.*]) during the encounter on October 26, 2004 (TA flyby), crossing the Titan's tail approximately in the similar location as the Voyager 1. Ionospheric ion and electron temperatures were taken from model calculations of *Roboz and Nagy*, [1994]: T_I = 0.035 *eV*, $T_{e,cold}$ ~ 2 T_I. The mass of the dominant ionospheric ion species was taken to be m_I = 28 AMU (possibly $C_2H_5^+$, $H_2CN^+$and N_2^+, according to ionospheric composition models of *Keller et al.*, [1994], *Roboz and Nagy*, [1994], *Cravens et al.*, [1998]). External magnetic field was taken to be B_0 = 5 *nT* [*Nees et al.*, 1982]. The growth rate (solid line) and the wave number (dotted line) of the most unstable mode corresponding to a given wave propagation angle, θ = arccos($k_{||}/k$) calculated according to (1) is plotted as a function of the dominant mode frequency. The diamonds and squares show the values of the growth rates and wave numbers, respectively corresponding to the most unstable mode

obtained in the numerical simulation for different and fixed propagation angles listed in the figure. As can be seen, analytical and simulation results are in good agreement.

3.2 MTSI wave energy density

Next we investigate the total MTSI wave energy density, normalized to the total initial kinetic energy of the charged particles. The wave energy of the dominant mode was approximated by the following formula (*Styx*, [1992]):

$$W_{waves} = \sum_k \frac{\partial}{\partial \omega_k}\left[\omega_k \varepsilon_{xx}(k,\omega_k)\right]\frac{|E_{xk}|^2}{8\pi} \approx 6\frac{\omega}{k u_e}\left(\frac{\omega_{pe}}{\omega_{ce}}\right)^2 \frac{|E_x|^2}{4\pi} \qquad (3)$$

Here we have made use of the fact that the MTSI waves are predominantly electrostatic ($E_x >> E_y, E_z$). In Figure 3 we show the wave energy evolution in time at different propagation angles ($\theta = 88.5^0$: solid line, $\theta = 86.5^0$: dotted line, $\theta = 84.5^0$: dashed line). The plasma parameters (number densities, bulk velocity and thermal energy) corresponding to different charged particle populations are chosen close to those determined by Voyager 1 characteristic to the unperturbed magnetospheric plasma in the vicinity of Titan. As it can be seen from the Figure 3., the wave energy, after saturation, reaches a few percent of the total initial kinetic energy, its variation is mainly due to the kinetic energy of the transverse electron oscillation (introduced by factors of order of $(\omega_{pe}/\omega_{ce})^2 \sim \cdot 2\times 10^3$), and decreases with decreasing wave propagation angle.

3.3 Phase space density evolution

The evolution of the phase space density plots gives a deeper insight how the interaction really builds up. In Figure 4. we have displayed the phase space plots of beam protons (upper panels), oxygen ions (middle panels) and heavy ionospheric ions (lower panels) corresponding to times at the beginning of the nonlinear phase, $t\omega_{LH}$ = 30 (Figure 4a.; left panels) and at the turbulent phase, $t\omega_{LH}$ = 100 (Figures 4b.; right panels). The plasma parameters used are identical used the case of Figure 3., corresponding to propagation angle of $\theta = 84.5^0$. Velocities in the x direction are normalized to the proton thermal velocity, and distances to $\rho^* = (v_{Tp}/\omega_{ce})^{1/2}$. The vortex formation indicates that the nonlinear stabilization of the MTSI is mainly due to electrostatic trapping of the ionospheric ions and beam protons in the potential troughs of the large amplitude waves. At the beginning of trapping the large amplitude waves are almost monochromatic. As the first particles are trapped they begin to rotate with frequencies depending on the initial kinetic energy, leading to wave steepening and phase mixing. It is interesting to note the lack of substantial beam nitrogen / oxygen ion trapping, which is mainly due to their initial kinetic energy much larger than that of proton or ionospheric ion population. The condition of particle trapping, the level of wave energy saturation and the development of the initially monochromatic large amplitude wave into well developed plasma turbulence is discussed in section 4.

The effect of random particle acceleration by waves can also be illustrated by the change of ion velocity distribution function during the time evolution of the MTSI instability, shown in Figure 5. In case of the beam protons (Figure 5a.) a plato is formed in the velocity space around the wave-particle resonance velocities due to particle trapping and consecutive phase mixing. In the case of the 28AMU pickup ions a significant broadening and extended energetic tail formation of the velocity distribution can be observed (Figure 5b.) ion velocities growing to values

comparable to the decelerated proton beam velocity, order of few tens of *km/s*, in the direction of wave propagation.

3.4 Bulk momentum coupling, laminar pickup

It is possible to derive from the model the momentum coupling mediated by the MTSI waves between beam protons and O^+/CH_4^+ and initially stationary 28AMU ionospheric ions. This is exhibited in Figure 6. All other initial plasma parameters are the same as in Figure 3. The effectiveness of coupling depends on the saturated wave energy level and correspondingly decreases with decreasing angle between the external magnetic field and bulk plasma velocity. Protons and nitrogen / oxygen ions act passively to the instability during the linear growth stage (in agreement with the linear theory), however, beam ions start to exchange momentum and energy with waves when the wave electric field increases to levels at which particle trapping becomes effective. Protons and nitrogen / oxygen ions start to decelerate, and the bulk momentum lost is transferred to the stationary ionospheric ion population present within the interaction region. Protons loose a significant portion of their initial bulk momentum; and may even stop and change their initial flow direction (see Figure 6a). This effect may possibly be observed by the ion detectors of Cassini spacecraft as a proton depletion region, also called mass loading boundary in case of Mars plasma mantle. Due to their significantly higher thermal energy the 14-16 AMU ions can hardly be trapped by the wave electric field, thus loosing insignificant portion of their initial bulk momentum, however, this amount is still comparable to the total amount of momentum lost by the protons due to the large difference in mass (see Figure 6b). Stationary ions gain significant fraction (up to 10-15%) of the total initial bulk momentum of the streaming ion beam (see Figure 6c.) within distances much less

than the $E \times B$ type ion pickup energization. Since in our case momentum exchange between the different plasma populations is mediated by waves, and collective electromagnetic forces act as some kind of anomalous resistivity, we call this type of interaction as ***laminar ion pickup***. An estimation of the characteristic distance of laminar ion pickup is given in the next section.

Next we have presented the time history of the bulk velocity of the beam protons and picked up ionospheric ions (see Figure 7a) and the *rms* value of wave electric field (see Figure 7b) corresponding to different initial drift velocities of the ion flow impinging the ionosphere. For better comparison with the measurements we expressed these quantities in physical units. Results for three initial drift velocity values are presented: 1) U_b = 60 *km/s* (solid line), representing the case when Titan is within the magnetoshere of Saturn and the spacecraft is within the flowside mantle, near to the stagnation point of the corotational plasma flow; 2) U_b = 120 *km/s* (dotted line) is the value measured by Voyager 1 and Cassini within the wake region of Titan; and 3) U_b = 280 *km/s* (dot-dashed line) representing the case when Titan leaves the magnetospere of Saturn and is exposed directly to the solar wind. In the first two cases the magnetic field, ion density and temperature values were chosen to be identical to the ones used in the case of Figure 2, in the third, "solar wind" case we have chosen values for interplanetary magnetic field intensity, solar wind proton density and temperature estimated by *Wolf and Neubauer*, [1982]: $B_{IMF} \sim$ 1-2 *nT*, $n_p \sim$ 0.1 cm^{-3} and $T_p \sim$ 7-8 $\times 10^7$ *K* , respectively. In the case when U_b = 120 *km/s* we have also performed model calculations for lower beam ion temperatures measured by Cassini near the wake of Titan: $T_p \sim$ 50 *eV* , $T_{N/O+} \sim$ 1.0 *keV* (dashed line). The simulation results shown here correspond to propagation angles close to the fastest growing mode.

As one can expect, the pickup ion drift velocity increases with increasing initial beam drift energy from a stationary stage up to few *km/s*. This velocity is not enough

for bulk assimilation since it is well below the incoming beam drift velocity of magnetospheric or solar wind origin. On the other hand the protons may decelerate to below one tenth of its initial bulk velocity. The bulk velocity of the 14-16 AMU beam ions – not shown here - hardly changes via wave-particle interactions due to the lack of significant particle trapping, as explained in section 4. As it can be seen from Figure 6a, no considerable beam ion temperature dependence of the bulk velocity change was found: similar values of bulk velocity drop resulted in case of proton temperatures of 50 and 200 *eV* and 16 AMU ion temperatures of 1 and 3 *keV* .

We have also investigated whether the shape of the initial particle velocity distribution of the heavier beam ion component has any effect on the evolution of the instability. We compared Maxwellian distribution versus shell-distribution function shapes with comparable characteristic velocity space width (simulation result are not shown in Figure 7a.), and found no significant difference between the different cases.

The root mean square average intensity of the dominant wave electric field component, $E_x^{rms} \propto \sqrt{\int E_x^2 d\omega}$ increases and saturates at few tens of *mV/m* (see Figure 7b.), proportionally with the increase of the initial kinetic beam energy. Using cooler beam ion temperature or shell/ring shaped velocity space distribution function did not change the final wave energy level significantly.

In the linear growth stage the characteristic frequency of the dominant MTSI mode is somewhat below the local lower hybrid frequency, ω_{LH}, as shown in Figure 2., and is of order of or below 1 *Hz* within the plasma mantle of Titan (according to model calculations presented by *Dóbé and Szego* [2005]). During the nonlinear evolution of the instability the trapped ions initially are bunched together within the potential well of the wave electric field, resulting in wave overtaking and saturation of the high amplitude, almost monochromatic, nonlinear MTSI electrostatic waves. Subsequently, phase mixing of the trapped ion motion takes place, and the wave

spectra significantly broadens up to few times of the lower hybrid frequency. This mechanism is explained in more details in section 4.

3.5 Stochastic ion heating

Nonlinear interaction between waves and particles also results in significant heating of the trapped ions. In Figure 8. we have presented the time history of the random kinetic (ie. thermal) energy content of the beam protons and the initially cold, 28AMU ions of ionospheric origin corresponding to three different initial beam velocity values normalized to the proton thermal velocity: $u = U_b/V_{thp} = 0.5$, 1 and 2, respectively, where $V_{thp} = \sqrt{T_p/M_p}$. Again, wave propagation directions were chosen close to the fastest growing mode. The thermal energy of beam 16AMU ions – not shown here – does not change significantly, due to the lack of significant particle trapping. As we can see from the figure, the saturated thermal energy monotonically increases with increasing initial beam drift energy for both ion types. The energy contained within the random motion of protons may grow by up to 130% (Figure 8a) of the initial proton thermal energy ($T_p \sim 210$ eV). An even more pronounced ion heating takes place within the ionospheric ion population (Figure 8b.), resulting in more than 6000 times higher thermal pickup ion energy compared to the initial thermal energy levels ($T_i \sim 0.035$eV).

3.6 Pickup ion mass dependence

We also investigated the effect of the pickup ion mass onto the final saturation level of the wave energy, and pickup ion energization. Figure 9. shows the effect of pickup

ion mass variation on the time evolution of the instability. Three generic ion species were included in the model calculations: light (~1 AMU mass, e.g. H^+), medium (~16 AMU mass, e.g. O^+ or CH_4^+) and heavy (~ 28 AMU mass, e.g. N_2^+ or H_2CN^+) species. It can be seen from Figure 9a. that the MTSI wave fluctuation level at the breakdown of wave energy growth and the final saturation level does not depend on the pickup ion mass very strongly. On the other hand Figure 9b. shows that in case of the pickup protons the complete thermalization occurs faster (at times of about 60-70 ω_{LH}^{-1}), and at lower saturated thermal energy levels (fraction of percent of the total kinetic energy) compared to the case of the higher mass pickup ion species (after times of 150 ω_{LH}^{-1} and at energy levels of order of few percent). The rate of thermal energy change decreases with increasing pickup ion mass, due to smaller oscillating frequency and corresponding phase mixing rate of the pickup ions trapped within the electric potential wells of the waves.

4. A few important issues concerning the model results

4.1 Evolution of the wave energy

There are a few results presented in the previous section that deserves further analysis. The first is the evolution of the wave energy. In the previous section it was shown that after the linear growth stage the monochromatic large amplitude MTSI waves lose their resonance with the beam and saturate by particle trapping. The plasma wave energy may grow up to few percent of the total kinetic energy, reaching *rms* electric field intensities of 5-35 *mV/m*. Simulation results also showed that the

maximum and saturated wave amplitudes decrease with decreasing angles between the magnetic field and beam velocity vectors, and saturation wave energy also scales with the initial beam kinetic energy.

The saturated wave energy level determined by particle trapping can be estimated in the following way. The magnitude of wave potential needed for electrostatic particle trapping of the unmagnetized ions to be started can be given by the following well known resonance condition: $\Delta v = |v - v_{ph}| \leq (e\varphi_T/m)^{1/2}$, where $v_{ph} = \omega/k$ is the phase velocity and φ_T is the wave potential at which the ions start to trap. During the linear and nonlinear growth stage of the MTSI instability the phase velocity of the waves is much smaller than the drift velocity of the beam. For example, in case of beam velocities and propagation directions corresponding to $U_b \sim v_{Tp}$ and $\kappa = 9$ – using the analytic approximation (2) – $\omega/k \sim (½)^{4/3} (n_i/n_e)^{1/3} (m_p/m_I)^{1/3}(n_b/n_e) U_b /\kappa^{2/3} \sim 0.012$ v_{Tp}. In case of protons only the low velocity part of the distribution can be trapped, as shown by the well-developed vortices in Figure 4a.; upper panel. Due to their higher mass and, correspondingly, higher kinetic energy the beam nitrogen / oxygen ions need higher wave electric fields for being effectively trapped, so their phase space vortices are absent or less pronounced. In case of the cold ionospheric ions the phase velocity initially fell outside the bulk part of the stationary ion velocity distribution: $\omega/kv_{Ti} \sim 5$. However, by the end of the linear growth phase of the instability ($t\omega_{LH} \sim 30$) the bulk velocity of the ionospheric ions increased to the order of the phase velocity of the MTSI waves, as shown in Figure 6a., and the ions can be also trapped in large numbers.

4.2 Ion trapping mechanism

It is worthwile to look into the details how ions get trapped. Since the trapped particles are continously reflected by the wave potential, they exhibit periodic motion within the wave potential troughs. The difference existing in the oscillation period (function of initial kinetic energy) and initial phase of trapped particle motion causes density bunching within the phase space (seen in Figure 4a.), and strong harmonic distortion ("steepening") of the large amplitude, initially monochromatic wave form. Particles moving faster than the wave transfer energy to the wave, while slower particles gain energy from the wave, leading to oscillation of the electric field energy density (see Figure 3.) with periods determined by the bounce frequency of the particles, defined as $\omega_B = (ek_{max}E_{sat}/m_i)^{1/2}$, where k_{max} is the wave number of the dominant wave mode, and E_{sat} is the maximum, saturated amplitude of the wave electric field. In the long run the number of the two particle populations equalizes, and the energy exchange between the resonance particles and waves is turned off.

The growth of wave electric field stopes and the wave saturates when the cohenrently moving bunches of trapped particles first reverse their motion within the wave potential trough. The ionospheric ions act as a coherent beam with small velocity spread within the wave reference frame. After most of the ions being trapped and rotated in the phase space the saturated wave energy for the dominant instability mode may be approximated by the following expression (*Drumond et al.*, [1970]):

$$W_{sat}^{Ions} \approx n_I m_I \left(\frac{\omega_{\max}}{k_{\max}}\right)^2 \approx \frac{1}{2^{5/3}} \left(\frac{n_i}{n_e}\right)^{5/3} \left(\frac{m_I}{m_p}\right)^{1/3} \frac{n_e m_p U_e^2}{\kappa^{4/3}} \qquad (4)$$

In case of the protons only a part of the beam is in resonance with the initially monocromatic wave. In this case the saturation is determined by the usual expression of finite resonance width of the growing wave spectrum: $\Delta v = |v - \omega/k| \sim \gamma_{max}/k_{max} \sim$

$(e\varphi_{sat}/m)^{1/2}$. For the dominant mode using (2) we can approximate the wave energy saturated by beam protons as:

$$W_{sat}^{protons} \approx 6\frac{\omega}{ku_e}\left(\frac{\omega_{pe}}{\omega_{ce}}\right)^2 \frac{(k_{\max}\varphi_{sat})^2}{4\pi} \approx 0.53\left(\frac{n_i}{n_e}\right)^{5/3}\left(\frac{m_p}{m_I}\right)^{5/3} \frac{n_e m_p U_e^2}{\kappa^{4/3}} \qquad (5)$$

It can be seen that in the case of both ion types the saturated wave energy monotonically decreases with increasing κ (i.e. decreasing wave propagation angle relative to the external magnetic field, in agreement with the results presented in Figure 3) following the same power law dependence, and also scales with the initial beam drift velocity. However, the saturated value of the wave energy density is of order of $(m_I/m_p)^2$ times higher in case of the ionospheric ions trapping compared to the value determined by trapped beam protons only. A comparison of the analytical estimations (3) and (4) to the simulation results shows that the saturated wave energy level is mainly determined by the trapping of the ionospheric ion population by the large amplitude monocromatic MTSI wave.

It is also interesting to note that the final fluctuation level at saturation does not depend very strongly on the ionospheric ion mass (see Figure 9a). This behavior may be attributed to the fact that the estimated wave energy density at the breakdown of the instability growth phase – according to (3) – is proportional to $(m_I/m_p)^{1/3}$. This means that the relative difference between the saturation wave energy corresponding to ion species is relatively small: $W_{sat}^{28AMU} = 1.26\ W_{sat}^{14AMU} = 3.04\ W_{sat}^{1AMU}$

4.3 Wave spectrum broadening, side band instability

Another important consequence of ion trapping and oscillatory motion is the rapid broadening of the initially almost monochromatic wave spectrum. The trapped particles oscillating in the wave trough are able to act coherently like a beam and produce something similar to a two stream instability, called side-band instability (*Kruer et al.*, [1969], *Shapiro and Schevchenko*, [1988]). These side band waves are excited against the background of the main MTSI wave, being in resonance with the *n*th harmonic of oscillatory motion of the trapped particles. The effective resonance condition may be written as:

$$\omega_{SB} - k_{SB} v_{ph} \approx \pm n \omega_B(\varepsilon) \qquad (6)$$

where ω_{SB} and k_{SB} is the frequency of the sideband instability mode in the Titan's reference frame, $\omega_B(\varepsilon)$ is the energy dependent bounce frequency of the trapped particles, $\varepsilon < (eE_x^{max}/k_{max})$; v_{ph}, k_{max} and E_x^{max} are the phase velocity , wave number and amplitude of the dominant monochromatic wave electric field parallel to the direction of propagation. In Figure 10. we have shown the Fourier spectra of the wave electric field corresponding to two different evolution stages of the instability: linear and nonlinear growth (see Figure 10a.) and turbulent phase (see Figure 10b.), corresponding to case when the initial beam drift velocity is $U_b = 2v_{tp}$. As we can see from Figure 10a. at the end of the linear growth stage, when significant number ionospheric ions got trapped into potential wells of the waves, the main MTSI wave becomes unstable and significant energy got pumped into another mode with somewhat higher frequency and wave number which we identify to a sideband instability mode. According to (5) the frequency shift corresponding to the $n = 1$ case may be approximated as $\Delta\omega = \omega_{SB} - \omega_{MTSI} = \alpha\ (eE_x^{max} k_{MTSI}/m_I)^{1/2}$ where α is a number of order or less than unity, ω_{MTSI} is the frequency of the dominant linear

MTSI mode, and we could also made use of the approximation $k_{SB} \approx k_{MTSI}$. In case of $U_b = 2v_{tp}$ by using the corresponding electric field amplitude ($E_x^{max} \sim 15mV/m$) and wave number ($k_{MTSI} \sim 1.4\ 10^{-3}\ m^{-1}$) values one can obtain for the frequency shift an approximate shift of $\Delta\omega \sim 0.4\ \omega_{LH}$, which is in agreement with the frequency shift of the new instability branch shown in Figure 10a. Moreover, $k_{SB} - k_{MTSI} \sim 0.12\ k_{MTSI}$. As the instability further evolves new generations of sideband instability modes are excited, which together with the phase mixing of the trapped particles and nonlinear wave-particles effects the wave spectrum broadens, as seen in Figure 10b, pumping significant energy in frequency ranges of several times the lower hybrid frequency. Using the typical background plasma and magnetic field values introduced in case of Figure 2., we obtain for lower hybrid frequency, $\nu_{LH} \sim 3\ Hz$, thus the nonlinearily broadened wave frequencies may reach values of order 6-9 *Hz*.

Another important consequence of the generation of the sideband instability modes is that as a result of the superposition of the MTSI and sideband instability modes a beat wave mode appears which propagates at phase velocity $v_{ph}^{Beat} \sim (\omega_{SB}-\omega_{MTSI})/(k_{SB}-k_{MTSI}) \sim 0.25v_{Tp}$. This phase velocity being much larger than the propagation speed of the MTSI waves ($v_{ph}^{MTSI} \sim 0.05v_{Tp}$) , falls well within the distribution function of the protons. This leads to a more rapid proton trapping and also since protons are more effectively scattered on the beat waves (nonlinear Landau damping) than on the primary MTSI waves their motion can be "collectivized" resulting in a more effective plato formation in the velocity space toward velocities in the vicinity of the phase velocity of the waves and accordingly a more effective heating.

4.4 Effectiveness of the energy and momentum exchange

One of the primary effects of the wave-particle interaction due to a particular instability is to reduce the source of free energy driving that instability, in our case the kinetic energy of the beam. It is particularly important to evaluate the energy exchange rate between the plasma components moving relatively to each other. After saturation of the MTSI instability by trapping of a significant part of both beam and ionospheric ions, the motion of the trapped particles becomes stochastic within the large amplitude wave potential troughs, the initially close to monochromatic wave spectrum significantly broadens, and the quasilinear approach becomes applicable. According to the quasilinear approximation a balance between the linear growth and nonlinear wave damping is maintained into the post-saturation phase, during which the enhanced fluctuations scatter the plasma particles. This scattering may be conceived as an "anomalous" particle transport within the phase space, and the associated wave-particle energy exchange rate can be described by the so called the effective collision frequency (see for example *Rosenbluth and Sagdeev*, [1984]). According to this picture in equilibrium the average momentum loss of the charged particles has to be transferred to the random phase waves modes (plasmons) emitted by particles in unit time, and the effective collision frequency may be defined as:

$$\nu_{eff} = \frac{1}{P_b}\int d^3k \gamma_k W_k \frac{\mathbf{k}\cdot\mathbf{U_b}}{\omega_k U_b} \qquad (7)$$

where P_b and U_b is the drift momentum and beam drift velocity of the beam, respectively; W_k and γ_k is the spectral energy density and growth rate of the MTSI waves in the quasilinear phase, respectively.

The physical meaning of this expression is that the rate of momentum loss of the beam balanced by the rate of plasmon generation induced by the instability.

In our case we can argue that the most unstable mode of the MTSI instability propagates in the direction of the drift velocity, so (6) can be further simplified using (2) and (4) leading in the one dimensional case to the expression:

$$\nu_{eff} = [\gamma_k (k/\omega_k) W_k]_{max}/P_b \quad (8)$$

These expressions are applicable only after the motion of plasma particles had been "collectivized", and the quasilinear approximation may be used. In our case the dominant part of the beam momentum density is given by the nitrogen / oxygen ions. Assuming that the wave energy may be determined by the formula (3), one can approximate the effective collision frequency corresponding to the most dominant wave mode. Using the plasma parameters measured by the Voyager-2 within the wake of Titan and wave energy density corresponding to the dominant mode obtained by the simulation in this case ($n_i = n_{beam}$=0.3 cm^{-3}, m_i=28AMU, m_{beam} ~ 14 AMU, U_b=120 km/s, E_x=5 mV/m) finaly one can obtain for the effective collision frequency: ν_{eff} ~ 0.7 s^{-1}. One can also estimate the characteristic distance of the spatial diffusion of the ionospheric ions as $L \sim U_b/\nu_{eff}$ ~ 150 km, which more than an order of magnitude smaller than the length scale needed for an effective $E \times B$ pick-up determined by the gyromotion of the ionospheric ions (having a gyroradius of about ~ 2500 km). This result suggests that the MTSI mode provides an effective coupling between the corrotation plasma of Saturn and ionospheric plasma of Titan.

5. Comparison of the simulation results with Cassini CASP measurements

Cassini Plasma Spectrometer, CAPS (Young et al., [2004]), flying onboard Cassini, has three independently operated sensors: the ion mass spectrometer (IMS) designed

to analyze ion composition and plasma dynamics, the electron spectrometer (ELS), and the ion beam spectrometer (IBS) to measure narrow, beam-like distributions without mass separation. The IMS covers the ion energy-per-charge range 1 V ≤ E/Q ≤ 50 keV, and the ELS has the electron energy range 1 eV ≤ E ≤ 28 keV. The whole CAPS package can be actuated around a rotation axis parallel to the symmetry planes of the IMS and ELS fields of view. IMS measures ion energy in 63 channels with logarithmically increasing energy steps up to ~50 keV in 8 elevation directions, each ~20^0 wide, the field of view in the azimuth direction was 11^0 (the azimuth direction is in the actuator plane, the elevation is perpendicular to it). The IMS allows to detect E/Q spectra of all ion species (not discriminating by mass), and also enabled to perform detailed compositional analyses using time-of-flight technique.

Significant slowing down of drifting magnetospheric plasma attributed to mass loading was observed by Voyager 1 and confirmed by Cassini in this region. The mass loading region was more extended in the anti-Saturn side (see *Crary et al.*, [2005]), where the motional electric field ($E = -U_b \times B$) pointed outward of Titan, and a rapid return to the dynamical conditions of Saturn's magnetosphere plasma was observed when the spacecraft left the ionosphere. *Hartle et al.,* [submitted to *Geophys. Res. Lett.*] showed that this asymmetry can be attributed to the fact that pickup ions born in the Saturnian side of Titan following their cycloidal trajectories can easily intercept Titan's atmosphere where most of them are absorbed. Several features of the interaction region of Titan observed by Cassini's ion mass spectrometer measurements performed within the interaction region of Titan are in good agreement with the simulation results. *Dóbé and Szego*, [2005] demonstrated that the MTSI waves may be feasible only in the presence of cold electrons of ionospheric origin, thus our result are applicable mainly in plasma regions just outside the ionosphere, close to the "ionopause".

Figures 11b and 12b illustrate the variation in time of the energy boundaries of ion count-energy spectra measured by CAPS during the flybys in the wake and flowside region of Titan, before closest approach (CA) during the TA encounter on October 26, 2004, and the same after CA during the T5 flyby on 16 April, 2005, respectively. During the TA encounter CAPS was actuating, during T5 the actuator was set to a fixed position along the ram direction; the patchy structure for TA is due to actuator motion. The spatial orientation of the two corresponding spacecraft trajectories are illustrated in figures 11b and 12b. As it can be seen from both figures significant decrease in the H^+ and H_2^+ characteristic energies occured in the anti-Saturnian side just before Cassini entered into the ionosphere. This can mainly be attributed to mass loading effects caused by $E \times B$ and/or laminar type pickup, the later mechanism being introduced in section 3.4. One of the main differences between the two pickup mechanisms is the characteristic distance needed for the ion energization. In case of $E \times B$ type pickup the characteristic scale length is of order of the gyroradius of the heavy ions of ionospheric origin, which characteristically is about 2000-3000 *km* within the plasma mantle of Titan. This distance is much larger than the characteristic momentum coupling distance mediated by MTSI waves, being of about 100-200 *km*, according to an analyses presented in section 4.4. The scale length of the laminar pickup is well within the distances needed for $E \times B$ type energization, demonstrating that the laminar pickup mechanism can be effective even within the physical dimensions of order of few hundred kilometers of the flowside plasma mantle of Titan.

Simulation results presented in the previous sections showed that the collective interaction between the charged particles and MTSI waves lead to both bulk and stochastic momentum and energy exchange between the moving magnetospheric and stationary ionospheric plasma. The beam proton bulk velocity values measured just above the ionopause are of the order of tenth of the magnetospheric plasma flow

velocities measured outside the mass loading region (as illustrated in figures 11b and 12b, and discussed by *Crary et al.*, [2005] and *Hartle et al.*, [submitted to *Geophys. Res. Lett.*]). These measured proton drift velocity drops are of the same order of magnitude as the simulated values shown in Figure 7a, where the proton beam decelerated from velocities of 60-120 *km/s* to final velocities of order of 8-25 *km/s*. The same anomalous friction type forces generated by wave-particle interaction can accelerate the heavy pickup ions to drift velocities of order of few *km/s*.

On the other hand the drift velocity of the heavy (14-16 AMU) ion beam component hardly changes since the particle trapping by the potential well of the beam generated MTSI waves is inefficient for ions with kinetic energies of order of keV. For more detailes of the particle trapping mechanism see section 4.2. According to *Sittler et al.*, [2004] and *Hartle et al.*, [submitted to *Geophys. Res. Lett.*] when Cassini was crossing the tail of Titan and approaching the ionosphere the signitures of the 14-16 AMU beam ions disappear due to the atmospheric capture of the background plasma.

In the case of the flowside plasma mantle crossing (shown in Figure 12b.) the signitures of the higher mass beam ions with characteristic energies of order of several kiloelectronvolts did not disappear within the proton decceleration region as it was observed during the tail crossing of Cassini. This may be attributed to the fact that the energetic ambient ions are gradually removed by atmosphere capturing due to finite giroradius effects when moving from the upstream towards the downstream interaction region. However, at this point is unclear why the count rates of the heavier beam ions increased just above the ionosphere relative to the count rates detected in the unperturbed magnetospheric plasma region.

In Figure 13. CAPS time-of-flight measurements are exhibited. Data were taken during flyby TA, between -912s and -656s, above the wakeside “ionopause” of Titan, in the region of magnetic field draping. *Hartle et al.*, [submitted to *Geophys.*

Res. Lett.] identified light ion signitures as mainly deccelerated magnetospheric protons, while 14 and 28 AMU ions are most probably pickup ions of ionospheric origin. According to our simulation results, the nonlinear wave-particle interaction transfers beam-directed energy into stochastic heating of the ions, and the distribution function broadens both for hydrogen and heavy pickup ions. This effect is especially pronounced in the case of the ionospheric ion population, where the energetic tail can reach velocities of order of 10-20 *km/s* (see figures 4 and 5), corresponding to energies of order of 15-60 *eV*. This energy range is in agreement with the pickup ion energies shown in Figure 13. Again, we need to point out that since these measurement were taken within the tail region of Titan, the energetic pickup ions detected above the ionopause may be accelerated to higher than thermal energies by the combined effects of the $E \times B$ type and laminar pickup ion effects.

Plasma waves were measured in the frequency range of interest, however, the data analysis requires more time due to various noise interferences (Kurth, private comm.); comparision of our results with the wave data will be possible only at a later stage.

6. Summary

We presented a one dimensional hybrid particle-in-cell simulation code retaining the inertia of the electrons to analyse the microphysics of the interaction between the corotational plasma flow of the magnetosphere of Saturn and the ionosphere of Titan. The interaction leads to excitation of mostly electrostatic waves with frequecies of the order of few *Hz* via modified two-stream-instability. The waves couple the external beam plasma to the ionosphreric ions typicaly within distances of 100-200 *km*. The coupling is very weak for the heavy (14-16 AMU) beam ion component, their energy

and momenta remain almost unchanged, whereas the light ion component of the flow, mainly protons loose most of their total momentum and bulk kinetic energy. The lost beam energy is transferred to the planetary ions through waves. As a result, these heavy pickup ions reach bulk velocities of order of few *km/s* and heated by nonlinear wave particle interaction to the temperature range of few tens of *eV*. The CAPS time-of-flight data were able to verify the most important conclusions of the model:

a) magnetospheric protons significantly deccelerate in the near ionopause region,
b) during flowside flyby the heavy component of the streaming magnetospheric ions did not loose their momenta,
c) planetary ions were accelerated and heated to superthermal energies.

The viscous-like interaction within the boundary layer between the ionosphere of Titan and the Saturnian magnetosphere, and strong energization of the ionospheric ions by nonlinear wave particle interaction effects may significantly contribute to the escape of the ionospheric plasma into the magnetosphere, and increase the continuous erosion of the atmosphere of Titan.

Acknowledgements.

References

Backes, H., F. M. Neubauer, M. K. Dougherty, N. Achellios, N. Andre, C. S. Arridge, C. Bertucci, G. H. Jones, K. K. Khurana, C. T. Russel, A. Wennmacher, Titan's magnetic field signature during the first Cassini encounter, *Science*, *308*, 992-995

Brecht, S. H. , J. G. Luhmann, and D. J. Larson (2000), Simulation of the Saturnine magnetospheric interaction with Titan, *J. Geophys. Res.*, *105*, 13,119–13,130

Chanteur et al. (2005), A 3-d hybrid simulation of the interaction region of Titan, talk presented at the Imperial College seminars on Titan

Crary, F. J., D. T. Young, R. A. Baragiola, B. L. Barraclough, J.-J. Berthelier, M. Blanc, M. Bouhram, A. J. Coates, J. T. Gosling, R. E. Hartle, T. W. Hill, R. E. Johnson, D. J. McComas, M. Michael, D. Reisenfeld, E. C. Sittler, H. T. Smith, J. T. Steinberg, K. Szego, M.F. Thomsen (2005), Dynamics and Composition of Plasma in and around Titan, submitted to *Science*, 2005

Cravens, T. E., C. J. Lindgren, and S. A. Lendvina (1998), A two-dimensional multi-fluid MHD model of Titan's plasma environment, *Planet. Space Sci.*, *46*, 1193–1206

Dóbé, Z., and K. Szego, Wave activity above the ionosphere of Titan: Predictions for the Cassini mission (2005), *J. Geophys. Res.*, *110*, A03224

Dóbé, Z., K. B. Quest, V. D. Shapiro, K. Szego, J. D. Huba (1999), Interaction of the solar wind with unmagnetized planets, *Phys. Rev. Lett.*, *83*, 260-263

Drumond, W. E., J. H. Malmberg, T. M. O'Neil and J. R. Thomson (1970), Nonlinear development of the beam-plasma instability, *Phys. Fluids*, *13*, 2422-2425

Gary, S. P., and N. Omidi, The ion/ion acoustic instability (1987), *J. Plasma Phys*., *37*, 45–61

Grebowski, J. M., W. T. Kasprzak, R. E. Hartle, K. K. Majahan, and T. C. G. Wagner (1993), Superthermal ions detected in Venus' dayside ionosheath, ionopause and magnetic barrier regions, *J. Geophys. Res*., **98**, 9055-9064

Hartle, R. E., E. C. Sittler, Jr., K. W.Ogilvie, and J. D. Scudder (1982), Titan's ion exosphere Observed from Voyager 1, *J. Geophys. Res*., *87*, 1383–1394

Hartle, R. E. , E. C. Sittler Jr., F. M. Neubauer[2], R. E. Johnson, H. T. Smith, F. Crary, D. J. McComas, D. T. Young, A. J. Coates, D. Simpson, S. Bolton, D. Reisenfeld, K. Szego, J. J. Berthelier, A. Rymer, J. Vilppola, J. T. Steinberg, N. Andre, Preliminary Interpretation of Titan Plasma Interaction as Observed by the Cassini Plasma Spectrometer: Comparisons with Voyager 1, submited to *Geophys. Res. Lett.*, 2005

Huba, J. D., Generation of waves in the Venus mantle by ion acoustic beam instability, *Geophys. Res. Lett*. (1993), *20*, 1751–1754

Kabin, K. P., P. L. Israelevich, A. I. Ershkovich, F. M. Neubauer, T. I. Gombosi, D. L. De Zeeuw, and K. G. Powel (2000), Titan's magnetic wake: Atmospheric or magnetospheric interaction, *J. Geophys. Res*., *105*, 10,761–10,770

Kallio, E., L. Sillanpaa, P. Janhunnen (2004), Titan's subsonic and supersonic flow, Geophys. Res. Lett., 31, L1 5703, doi: 10.1029/2004 GL 020344

Keller, C. N., T. E. Cravens, and L. Gan (1992), A model of the ionosphere of Titan, *J. Geophys. Res*., *97*, 12,117– 12,135

Kopp, A., and W.-H. Ip (2001), Asymmetric mass loading effect at Titan's ionosphere, *J. Geophys. Res., 106*, 8323-8332

Kruer, W. L., J. M. Dawson and R. N. Sudan (1969), Trapped-particle instability, *Phys. Rev. Lett.*, *23*, 838-841

Ledvina, S. A., and T. E. Cravens (1998), A three-dimensional MHD model of plasma flow around Titan, *Planet. Space Sci*., 46, 1175–1192

Lundin, R., A. Zakharov, R. Pellinen, H. Borg, B. Hultquist, N. Pissarenko, E. M. Dubinin, S. W. Barabash, I. Liede, H. Koshkinen (1989), First measurements of the ionospheric plasma escape from Mars, *Nature, 341*, 609–612

Ma, Y. J., A. F. Nagy, T. E. Cravens, I. G. Sokolov, J. Clark, and K. C. Hansen (2004), 3-D global MHD model prediction of the first close flyby of Titan by Cassini, *Geophys. Res. Lett.*, 31, L22803, doi: 10.1029/2004GL021215

Nagy, A. F. and T. E. Cravens (1998), Titan's ionosphere: A review, *Planet. Space Sci*, *46*, 1149-1155

Nagy, A. F., Y. F. Liu, K. C. Hanson, K. Kabin, T. I. Gombosi, M. R. Combi, D. L. deZeeuw, K. G. Powel, and A. J. Kliore (2001), The interaction between the magnetosphere of Saturn and Titan's ionosphere, *J. Geophys. Res.*, *106*, 6151-6160

Ness, N. F., M. H. Acuna, K. W. Behannon, and F. M. Neubauer (1982), The induced magnetosphere of Titan, *J. Geophys. Res.*, *87*, 1369–1381

Neubauer, F. M., D. A. Gurnett, J. D. Scudder, and R. E. Hartle (1984), Titan's magnetospheric interaction, in *Saturn*, edited by T. Gehrels and M. S. Matthews, pp. 760-787, Univ. of Ariz. Press., Tucson

Neubauer, F. M. (1991), Titan's magnetospheric interaction, *Proc. Symp. on Titan, Toulouse*, France, *ESA SP-338*, 267

Quest, K. B., V. D. Shapiro, K. Szego, Z. Dóbé (1997), Microphysics of the Venusian and Martian mantles, *Geophys. Res. Lett*., *24*, 301–304

Quest, K. B. (1989), Hybrid simulation, in *The 3rd International School for Space Simulation (ISSS-3): Tutorial Courses*, edited by Lembege, CRPE, Paris, pp. 172–182

Riedler, W., et al., (1989), Magnetic fields near Mars: first results, *Nature, 341*, 604-607

Rosenbauer, H., N. Shutte, I. Apáthy, A. Galeev, K. Gringauz, H. Grünwaldt, P. Hemmerich, K. Jockers, P. Király, G. Kotova, S. Livi, E. Marsch, A. Richter, W.

Riedler, T. Remizov, R. Schwenn, K. Schwingenschuh, M. Steller, K. Szego, M. Verigin, M. Witte (1989), Ions of martian origin and plasma sheet in the martian magnetosphere: initial results of the TAUS experiment, *Nature*, *341*, 612, 1989

Rosenbluth, M. N., and R. Z. Sagdeev (1984), eds. Handbook of Plasma Physics, North-Holland Physics Publishing

Roboz, A., and A. F. Nagy (1994), The energetics of Titan's ionosphere, *J. Geophys. Res*., *99*, 2087–2094

Sagdeev, R. Z., V. D. Shapiro, V. I. Shevchenko, A. Zacharov, P. Király, K. Szego, A. F. Nagy, and R. Grard (1990), Wave activity in the neighborhood of the bowshock of Mars, *Geophys. Res. Lett.*, *17*, 893–896

Sittler, E. C., R. E. Hartle, A. F. Viñas, R.E. Johnson, H. T. Smith, and I. Mueller-Wodard (2004), Titan Interaction with Saturn's Magnetosphere: Mass Loading and Ionopause Location, *Titan Book from Titan meeting at ESTEC*, April 13-17

Sittler, E.C., R. E. Hartle, A.F. Viñas, R.E. Johnson, H.T. Smith, and I. Mueller-Wodard, Titan interaction with Saturn's Magnetosphere: Voyager 1. Results Revisited, *J. Geophys. Res.*, *110*, A09302, doi:10.1029/2004JA010759, 2005

Scarf, F. L., W. W. L. Taylor, C. T. Russel, R. C. Elphic (1980), Pioneer Venus plasma wave observations: The solar wind-Venus interaction, *J. Geophys. Res*., *85*, 7599–7612

Shapiro, V. D., and V. I. Shevchenko, (1988), Astrophysical plasma turbulence I., *Sov. Sci. Rev. E. Astrophys. Space Phys.*, *6*, 425-546

Spenner, K., W. C. Knudsen, K. L. Miller, V. Novak, C. T. Russel, and R. C. Elphic (1980), Observation of the Venus mantle, boundary region between solar wind and ionosphere, *J. Geophys. Res*., *85*, 7655–7662

Spereiter, J. R. and S. S. Stahara (1985), Magnetohydrodynamic and gasdynamic theories for planetary bow waves, in: *Collisionless Shocks in the Heliosphere: Review of Current Research,* edited by B. T. Tsurutani and R. G. Stone, *AGU Geophys. Monograph, 35,* pp 85-108

Shapiro, V. D., K. Szego, S. K. Ride, A. F. Nagy, and V. I. Shevchenko (1995), On the interaction between the shocked solar wind and the planetary ions in the dayside of Venus, *J. Geophys. Res*., *100*, 21,289–21,298

Styx, T.H. (1992), *Waves in plasmas,* American Inst. of Physics, New-York.

Szego, K., Z. Bebesi, G. Erdos, L. Foldy, F. Crary, D. J. McComas, D. T. Young, S. Bolton, A. Coates, A. M. Rymer, R. E. Hartle, E. C. Sittler, D. Reisenfeld, J. I. Bethelier, R. E. Johnson, H. T. Smith, T. W. Hill, J. Vippola, J. Steinberg, N. Andre (2005), The global plasma environment of Titan as observed by Cassini Spectrometer during the first two close encounters with Titan, *Geophys. Res. Lett.*, *32*, L20S05, doi:10.1029/2005GL022646

Szego, K. K.-H. Glassmeier, R. Bingham, A. Bogdanov, A. Brinca, T. Cravens, E. Dubinin, Ch. Fischer, L. Fisk., T. I. Gombosi, G. Haerendel, M. Lee, Ch. Mazelle,

E. Mobius, U. Motschmann, P. Isenberg, V. D. Shapiro, K. Sauer, N. Schwadron, B. Tsurutani, G. Zank (2000a), Physics of Mass Loaded Plasmas, *Space Sci. Rev.*, *94*, 429-671

Szego, K., Z. Dóbé, J. Huba, K. Quest, and V. D. Shapiro, (2000b), Wave activity in the dayside mantle of Venus, Mars, and Titan, *Adv. Space. Res*., *26*, 1609–1612

Szego, K., Z. Dóbé, W. C. Knudsen, A. F. Nagy, V. D. Shapiro (1997), Energetic electrons in the dayside mantle of Venus, *J. Geophys. Res*., *102*, 2175–2183

Szego K., V. D. Shapiro, V. I. Shevchenko, R. Z. Sagdeev, W. T. Kasprzak, and A. F. Nagy (1991), Physical processes in the plasma mantle of Venus, *Geophys. Res. Lett.*, *18*, 2305–2308

Taylor, H. A., R. E. Daniell, R. E. Daniell, R. E. Hartle, H. C. Brinton, S. J. Bauer, and F. L. Scarf (1981), Dynamic variations observed in thermal and superthermal ion distributions in the dayside ionosphere of Venus, *Adv. Space Res*., *1*, 247–258

Young et al., Cassini Plasma Spectrometer Investigations, *Space Sci. Rev.*, *114*, 1-112, 2004

Wahlund, J.-W., R. Boström, G. Gustafson, D. A. Gurnett, W. S. Kurth, A. Pedersen, T. F. Averkamp, G. B. Hospodarsky, A. M. Persoon, P. Canu, F. M. Neubauer, M. K. Dougherty, A. I. Eriksson, M. W. Morooka, R. Gill, M. Andre, L. Eliasson, I. Müller-Wodarg (2005), Cassini measurements of Cold plasma in the ionosphere of Titan, *Science*, *308*, 986-989

Wolf, D. A., and F. M. Neubauer (1982), Titan's highly variable plasma environment, *J. Geophys. Res*., *87*, 881-885

Wu, C. S., Y. M. Zhou, S. T. Tsai, S. G. Guo, D. Winske, and K. Papadopoulos (1983), A kinetic cross-field streaming instability, *Phys. Fluids*, *26*, 1259–1267

Zang, T. L., J. G. Luhmann, and C. T. Russell, The magnetic barrier at Venus, *J. Geophys. Res.*, *96*, 11,145-11,153, 1991

K. Szego, MTA KFKI Reseach Institute for Particle and Nuclear Physics, H-1525 Budapest, POB 49, Hungary (szego@rmki.kfki.hu)

Figure 1. Schematic of the plasma environment of Titan illustrating the location of the flowside plasma mantle (upper panel), and the orientation of the coordinate system used during the model calculations (lower panel).

Figure 2. Real frequency (solid line) and wave number (dotted line) corresponding to maximum growth rate calculated according to the linear dispersion relation (1). Diamonds and squares correspond to simulation results determined in the linear growth phase of the MTSI instability, θ is the wave propagation angle relative to the magnetic field. Average beam plasma parameters are chosen close to the ones measured by Voyager 1 and Cassini in the plasma wake of Titan [*Hartle et al*., 1982; *Crary et al.*, 2005].

Figure 3. Linear and nonlinear evolution of the total MTSI wave energy density normalized to total initial kinetic energy corresponding to different propagation angles. All plasma and field parameters are identical to the ones used in case of Figure 2 and $\theta = 84.5^0$

Figure 4. Phase space distribution of protons (upper panels), 16 AMU ions (middle panels) and 28 AMU pickup ions at the saturation of the linear growth phase (left column), and the well developed turbulent phase (right column). All plasma and field parameters used are identical to the ones used in case of Figure 2 and $\theta = 84.5^0$.

Figure 5. Time history of beam proton (a) the 28 AMU pickup ion (b) distribution function. All plasma and field parameters used are identical to those used in case of Figure 2 and the propagation angle of the dominant mode, $\theta = 84.5^0$.

Figure 6. Evolution in time of the bulk momentum for beam protons (a), beam 16 AMU ions (b) and 28 AMU ionospheric ions (c) (each normalized to the total initial bulk momentum) corresponding to different wave propagation angles ($\theta = 88.5^0$ solid line, 86.5^0 dotted line, 84.5^0 dashed line, respectively)

Figure 7. Time history of the proton and picked up ionospheric ion drift velocity (a) and the *rms* value of the dominant MTSI wave electric field component (b) variation in function of initial beam drift velocity (U_{b0} = 70 *km/s*: solid line; U_{b0} = 140 km/s: dotted line; U_{b0} = 280 *km/s*: dashed line). All other plasma parameters taken are identical to those used in case of Figures 1, 2 and 3; fixed propagation angles do correspond to values close to the linear dominant mode.

Figure 8. Time history of thermal energy change of protons relative to the initial proton thermal energy (a); and thermal energy of picked up ionospheric ions relative to initial thermal energy (b) corresponding to different initial beam drift velocities (u_0 = U_{bo}/V_{Tp} = 0.5: solid line; = 1: dotted line; = 2: dashed line). All other plasma parameters taken are identical to those used in case of Figures 1, 2 and 3; fixed propagation angles do correspond to values close to the linear dominant mode.

Figure 9. Time history of the MTSI wave energy (a), proton beam momentum (b) and pickup ion thermal energy (c) in function of ionospheric pickup ion atomic mass (M_I = 1 AMU: solid line; M_I = 14 AMU: dotted line; M_I = 28 AMU: dashed line). All other plasma parameters taken are identical to those used in case of Figures 1, 2 and 3; propagation angle corresponding to the dominant mode: $\theta = 84.5^0$.

Figure 10. Fourier-spectra of the MTSI wave electric field parallel to the propagation direction at the end of the linear growth phase (a) and turbulent phase (b)

Figure 11. (a) Geometry of Cassini's TA encounter, crossing the wake region of Titan. The coordinate system is centered at Titan with the x axis pointing in the direction of Titan's orbital motion, y axes pointing toward Saturn, and the z axis being perpendicular to the orbital plane. The wake with respect to an ideal corotating plasma flow is also indicated. (b) The time variation in energy of the contours of count-energy spectra observed during TA before CA, in one (20^o wide) elevation channel of CAPS-IMS. The vertical axis shows time in sec relative to CA, the horizontal axis is energy in log eV units. The duration of one full energy sweep was 4 s; only the contour of the counts in the time-energy plot are of importance here; the patchy structure is due to the actuator motion. At the beginning of the time interval shown the light and heavy ion components of the corotational flow can be seen. The flow started to decelerate at about ~ –1400 s before CA (at about 10500 km from Titan), at this point the heavy ion components are lost in the exosphere. Cassini was in the ionosphere at about –300 s, the range of actuation was changed at –430 s before CA, and the actuation was centered around the ram direction.

Figure 12. (a) Geometry of Cassini's T106 encounter approaching Titan from the flowside direction. The coordinate system is the same as described in the case of Figure 11. (b) The time variation in energy of the edge enhanced contours of count-energy spectra observed during T5 after CA, in one (20^o wide) elevation channel of CAPS-IMS. One full energy sweep was taken in 4 s. The vertical axis shows time in sec relative to CA, the horizontal axis is energy in log eV units. The actuator pointed into the ram direction. At about 19:17, ~320 s after CA there was a discountinuity in the magnetic field. After that both the light and the heavy ion components of the

corotational flow can be seen partly in this channel of CAPS-IMS. The light ions of the flow started to decelerate at about 1000 s after CA, but the heavy ion component does not show any change in energy.

Figure 13. The time-of-flight spectrum taken between –912 *s* and –656 *s* before CA during TA, starting at 15:14:48 UT, in the region above the ionosphere of Titan. The vertical axis is energy per charge, E/Q [*eV*], the horizontal axis exhibits the ions resolved. The counts depicted by color are shown in logarithmic scale.

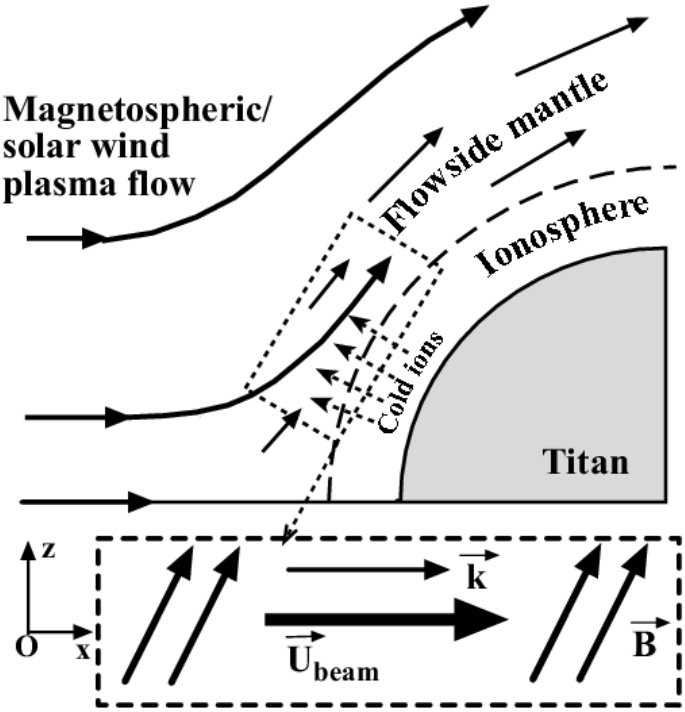
Magnetospheric/
solar wind
plasma flow
Flowside mantle
Ionosphere
Cold ions
Titan
z
O
x
k
U beam
B

Figure 1.

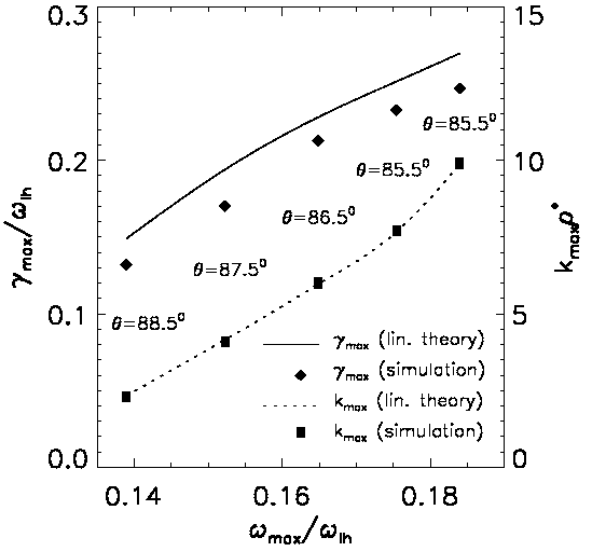
0.3
0.2
0.1
0.0
15
10
5
0
0.14
0.16
0.18
γ_{max}/ω_{lh}
$k_{max}\rho^*$
ω_{max}/ω_{lh}
θ=85.5°
θ=85.5°
θ=86.5°
θ=87.5°
θ=88.5°
γ_{max} (lin. theory)
γ_{max} (simulation)
k_{max} (lin. theory)
k_{max} (simulation)

Figure 2.

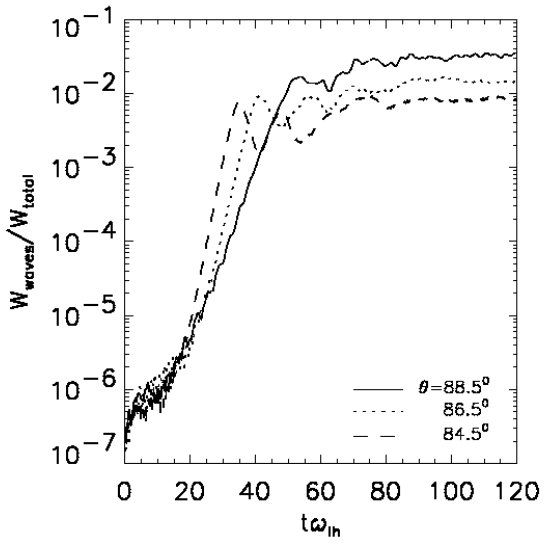
10^{-1}
10^{-2}
10^{-3}
10^{-4}
10^{-5}
10^{-6}
10^{-7}
W_{waves}/W_{total}
0
20
40
60
80
100
120
$t\omega_{lh}$
θ=88.5°
86.5°
84.5°

Figure 3.

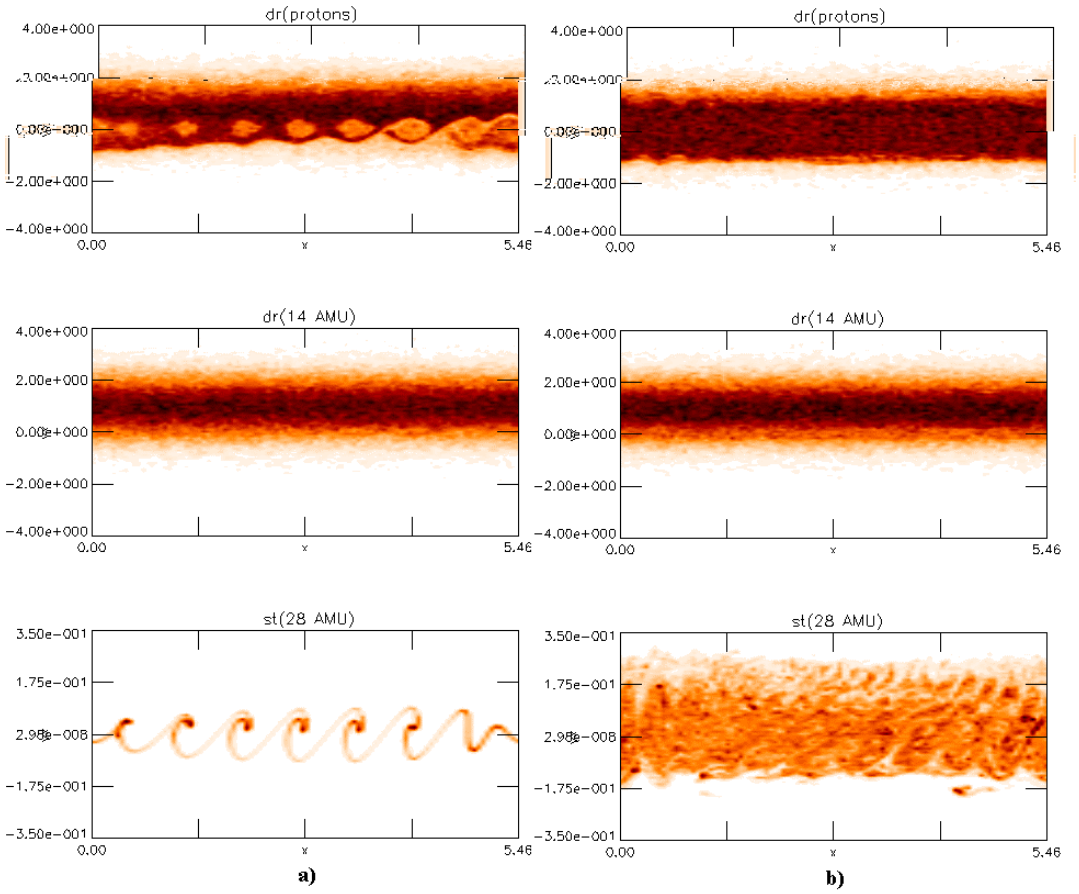
dr(protons)
4.00e+000
2.00e+000
0.00e+000
-2.00e+000
-4.00e+000
0.00
x
5.46
dr(protons)
4.00e+000
2.00e+000
0.00e+000
-2.00e+000
-4.00e+000
0.00
x
5.46
dr(14 AMU)
4.00e+000
2.00e+000
0.00e+000
-2.00e+000
-4.00e+000
0.00
x
5.46
dr(14 AMU)
4.00e+000
2.00e+000
0.00e+000
-2.00e+000
-4.00e+000
0.00
x
5.46
st(28 AMU)
3.50e-001
1.75e-001
2.98e-008
-1.75e-001
-3.50e-001
0.00
x
5.46
st(28 AMU)
3.50e-001
1.75e-001
2.98e-008
-1.75e-001
-3.50e-001
0.00
x
5.46
a)
b)

Figure 4.

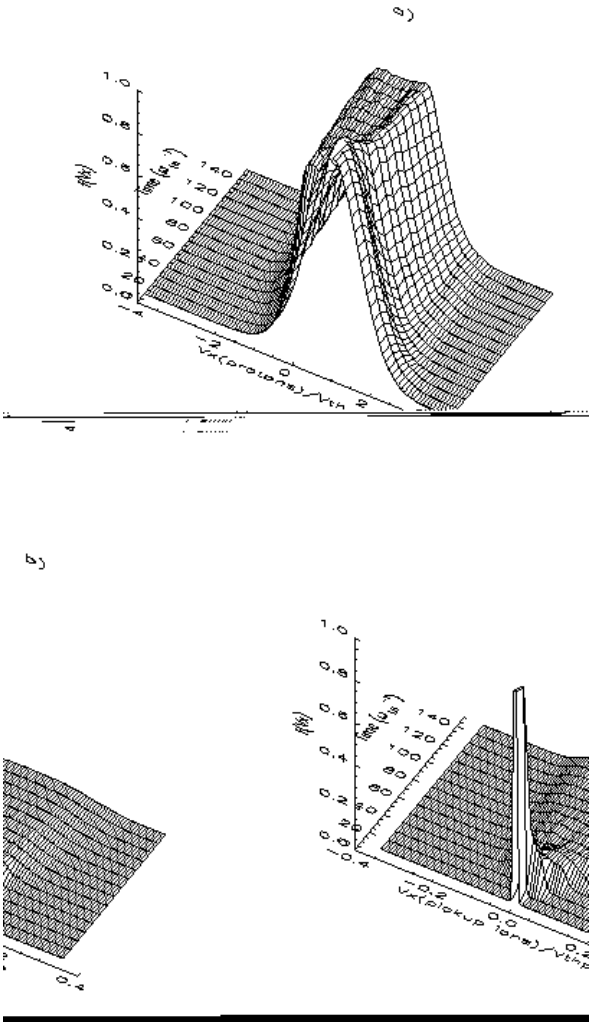

Figure 5.

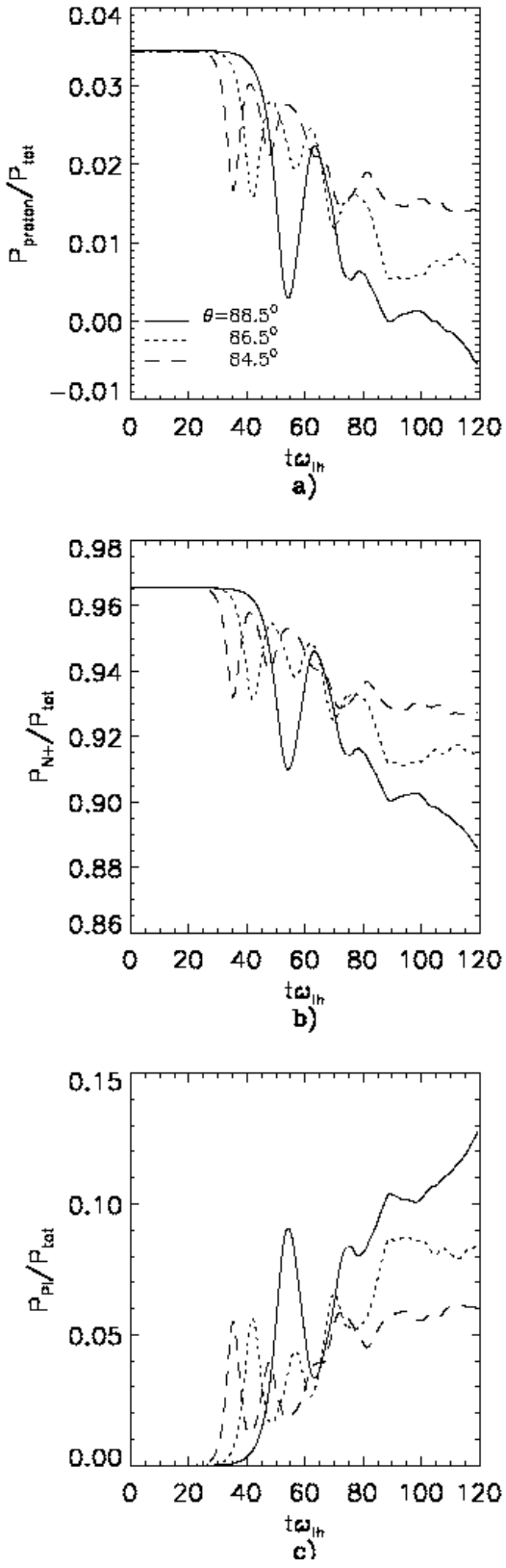
0.04
0.03
0.02
0.01
0.00
−0.01
P_{proton}/P_{tot}
θ=88.5°
86.5°
84.5°
0 20 40 60 80 100 120
$t\omega_{lh}$
a)
0.98
0.96
0.94
0.92
0.90
0.88
0.86
P_{N+}/P_{tot}
0 20 40 60 80 100 120
$t\omega_{lh}$
b)
0.15
0.10
0.05
0.00
P_{Pl}/P_{tot}
0 20 40 60 80 100 120
$t\omega_{lh}$
c)

Figure 6.

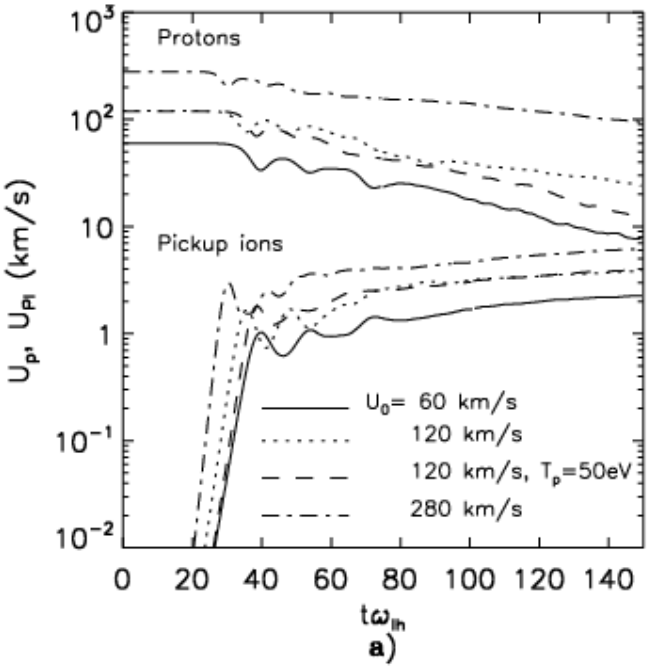
Protons
Pickup ions
U_p, U_{PI} (km/s)
U_0= 60 km/s
120 km/s
120 km/s, T_p=50eV
280 km/s
$t\omega_{ih}$
a)

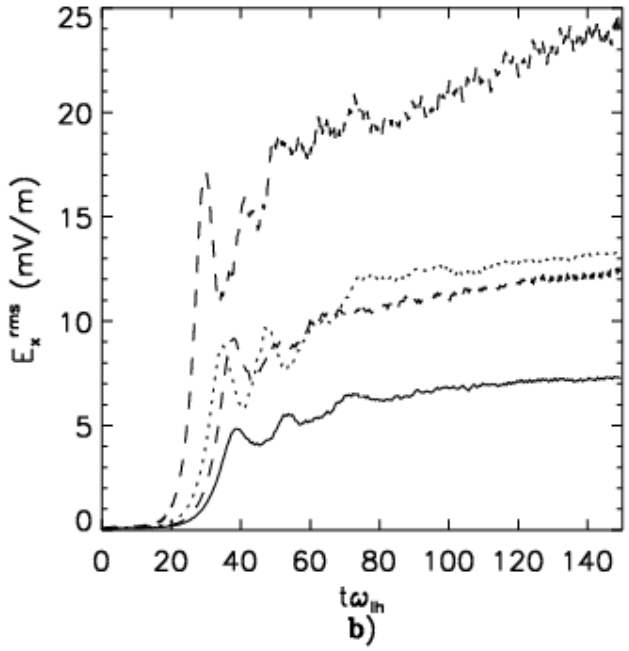
E_x^{rms} (mV/m)
$t\omega_{ih}$
b)

Figure 7.

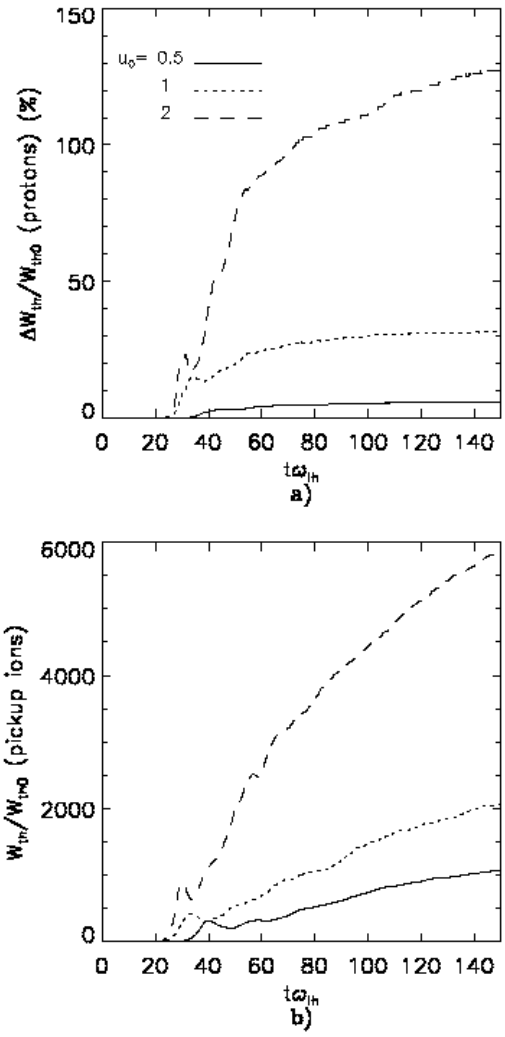
150
100
50
0
u_0= 0.5
1
2
$\Delta W_{th}/W_{th0}$ (protons) (%)
0 20 40 60 80 100 120 140
$t\omega_{ih}$
a)
6000
4000
2000
0
W_{th}/W_{th0} (pickup ions)
0 20 40 60 80 100 120 140
$t\omega_{ih}$
b)

Figure 8.

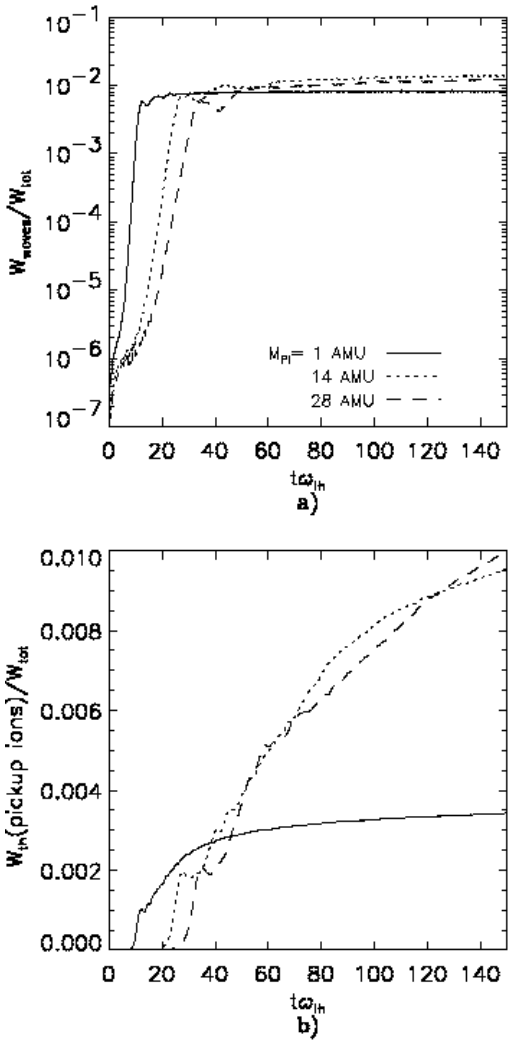
10^{-1}
10^{-2}
10^{-3}
10^{-4}
10^{-5}
10^{-6}
10^{-7}
W_{waves}/W_{tot}
M_{PI}= 1 AMU
14 AMU
28 AMU
0 20 40 60 80 100 120 140
$t\omega_{ih}$
a)
0.010
0.008
0.006
0.004
0.002
0.000
W_{th}(pickup ions)/W_{tot}
0 20 40 60 80 100 120 140
$t\omega_{ih}$
b)

Figure 9.

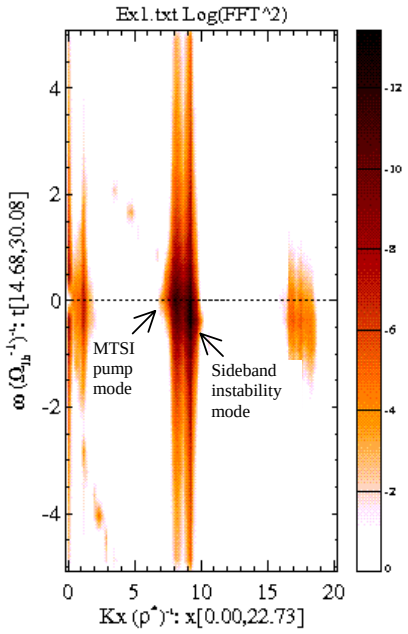
Ex1.txt Log(FFT^2)
MTSI
pump
mode
Sideband
instability
mode
Kx (ρ*)^-1: x[0.00,22.73]

a)

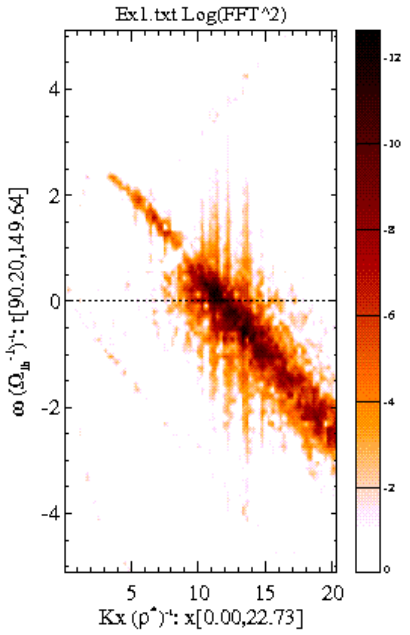
Ex1.txt Log(FFT^2)
Kx (ρ*)^-1: x[0.00,22.73]

b)

Figure 10.

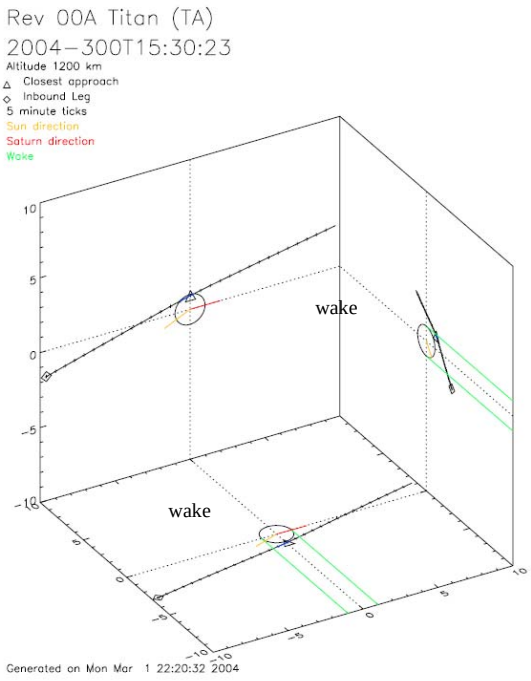
Rev 00A Titan (TA)
2004–300T15:30:23
Altitude 1200 km
Closest approach
Inbound Leg
5 minute ticks
Sun direction
Saturn direction
Wake
wake
wake
Generated on Mon Mar 1 22:20:32 2004

Figure 11a

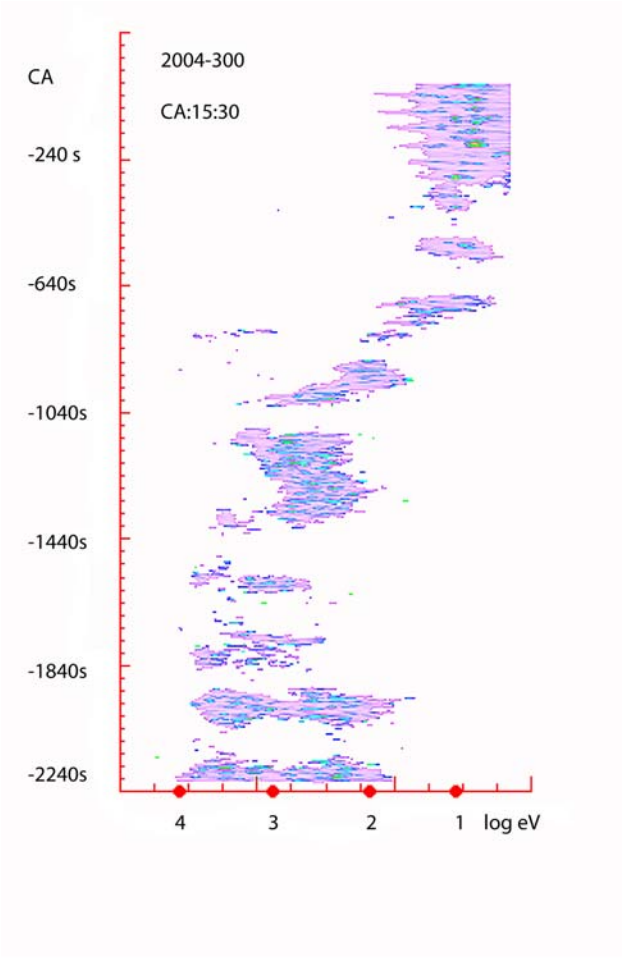
CA
2004-300
CA:15:30
-240 s
-640s
-1040s
-1440s
-1840s
-2240s
4
3
2
1
log eV

Figure 11b.

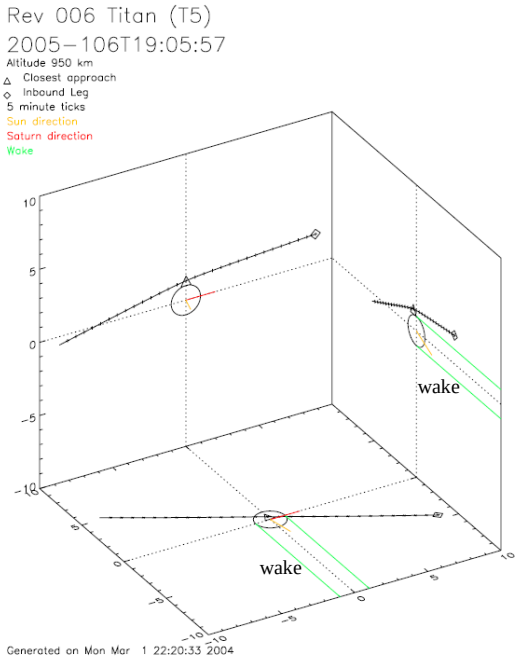
Rev 006 Titan (T5)
2005-106T19:05:57
Altitude 950 km
Closest approach
Inbound Leg
5 minute ticks
Sun direction
Saturn direction
Wake
wake
wake
Generated on Mon Mar 1 22:20:33 2004

Figure 12a

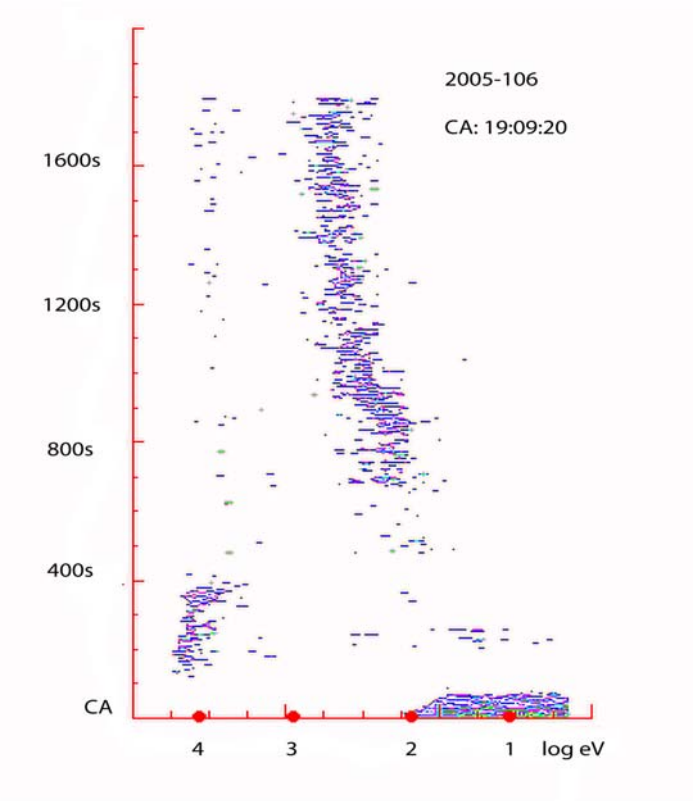

Figure 12b.

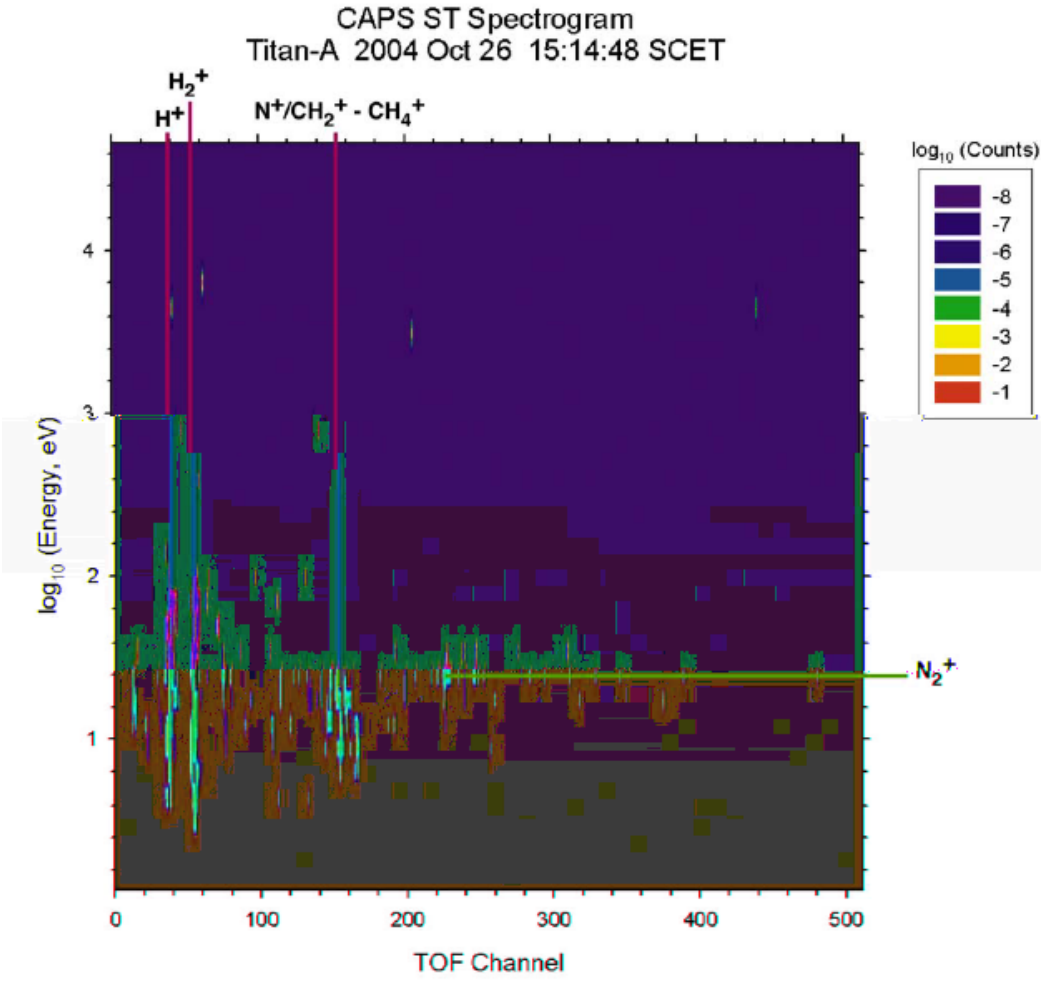
CAPS ST Spectrogram
Titan-A 2004 Oct 26 15:14:48 SCET
H2+
H+
N+/CH2+ - CH4+
log10 (Counts)
-8
-7
-6
-5
-4
-3
-2
-1
log10 (Energy, eV)
4
3
2
1
N2+
0
100
200
300
400
500
TOF Channel

Figure 13.